*Article*

# Effect of Nano-Graphene Oxide and n-Butanol Fuel Additives Blended with Diesel—*Nigella sativa* Biodiesel Fuel Emulsion on Diesel Engine Characteristics

**Hurmathulla Khan [1], Manzoore Elahi M. Soudagar [2], Rajagopal Harish Kumar [3], Mohammad Reza Safaei [4,5,6,*], Muhammad Farooq [7], Abdulqhadar Khidmatgar [8], Nagaraj R Banapurmath [9], Rizwan A. Farade [10], Muhammad Mujtaba Abbas [2], Asif Afzal [11], Waqar Ahmed [2], Marjan Goodarzi [12] and Syed Noeman Taqui [13]**

[1]  Department of Mechanical Engineering, HMS Institute of Technology, Tumkur 572101, India; h.khan@hmsit.ac.in

[2]  Department of Mechanical Engineering, Faculty of Engineering, University of Malaya, Kuala Lumpur 50603, Malaysia; manzoor@siswa.um.edu.my (M.E.M.S.); m.mujtaba@uet.edu.pk (M.M.A.); Hva180013@siswa.um.edu.my (W.A.)

[3]  Department of Mechanical Engineering, Sri Siddhartha Institute of Technology, Tumkur 572104, India; hodme@ssit.edu.in

[4]  Institute of Research and Development, Duy Tan University, Da Nang 550000, Vietnam

[5]  Faculty of Electrical—Electronic Engineering, Duy Tan University, Da Nang 550000, Vietnam

[6]  Center of Research Excellence in Renewable Energy and Power Systems, King Abdulaziz University, Jeddah 21589, Saudi Arabia

[7]  Research Centre for Carbon Solutions, IMPEE, Heriot-Watt University, Edinburgh EH14 4AS, UK; engr.farooq@uet.edu.pk

[8]  Department of Mechanical and Manufacturing Engineering, Faculty of Engineering, Universiti Putra Malaysia, Serdang, Selangor 43400, Malaysia; GS56631@student.upm.edu.my

[9]  Department of Mechanical Engineering, B.V.B. College of Engineering and Technology, KLE Technological University, Vidyanagar, Hubli 580031, India; nr_banapurmath@kletech.ac.in

[10]  Electrical Engineering Department, AIKTC School of Engineering and Technology, Panvel, Navimumbai 410206, India; rizwan.farade@aiktc.ac.in

[11]  Department of Mechanical Engineering, P. A. College of Engineering (Affiliated to Visvesvaraya Technological University Belagavi), Mangaluru 574153, India; asif_mech@pace.edu.in

[12]  Sustainable Management of Natural Resources and Environment Research Group, Faculty of Environment and Labour Safety, Ton Duc Thang University, Ho Chi Minh City 700000, Vietnam; marjan.goodarzi@tdtu.edu.vn

[13]  Department of Chemistry, University of Malaya, Kuala Lumpur 50603, Malaysia; noemansyed@siswa.um.edu.my

*  Correspondence: mohammadrezasafaei@duytan.edu.vn; Tel.: +1-502-657-9981

check for updates

**Abstract:** The present investigation uses a blend of *Nigella sativa* biodiesel, diesel, n-butanol, and graphene oxide nanoparticles to enhance the performance, combustion and symmetric characteristics and to reduce the emissions from the diesel engine of a modified common rail direct injection (CRDI). A symmetric toroidal-type combustion chamber and a six-hole solenoid fuel injector were used in the current investigation. The research aimed to study the effect of two fuel additives, n-butanol and synthesized asymmetric graphene oxide nanoparticles, in improving the fuel properties of *Nigella sativa* biodiesel (NSME25). The concentration of n-butanol (10%) was kept constant, and asymmetric graphene oxide nano-additive and sodium dodecyl benzene sulphonate (SDBS) surfactant were added to n-butanol and NSME25 in the form of nanofluid in varying proportions. The nanofluids were prepared using a probe sonication process to prevent nanoparticles

from agglomerating in the base fluid. The process was repeated for biodiesel, n-butanol and nanofluid, and four different stable and symmetric nanofuel mixtures were prepared by varying the graphene oxide (30, 60, 90 and 120 ppm). The nanofuel blend NSME25B10GO90 displayed an enhancement in the brake thermal efficiency (BTE) and a reduction in brake-specific fuel consumption (BSFC) at maximum load due to high catalytic activity and the enhanced microexplosion phenomenon developed by graphene oxide nanoparticles. The heat release rate (HRR), in-cylinder temperature increased, while exhaust gas temperature (EGT) decreased. Smoke, hydrocarbon (HC), carbon monoxide ($CO_2$) and carbon monoxide (CO) emissions also fell, in a trade-off with marginally increased $NO_x$, for all nanofuel blends, compared with *Nigella sativa* biodiesel. The results obtained indicates that 90 ppm of graphene oxide nanoparticles and 10% n-butanol in *Nigella sativa* biodiesel are comparable with diesel fuel.

**Keywords:** *Nigella sativa* biodiesel; graphene oxide nanoparticles; n-butanol; CRDI engine; performance and emission

---

## 1. Introduction

The rapid depletion of fossil fuels has led to renewable sources of energy gaining considerable attention [1]. One of the well-known and widely used renewable source of energy is biodiesel; biodiesel can be produced by using wide-ranging number of oils without any diesel engine modifications [2,3]. The feedstocks for biodiesel are generally classified as edible and non-edible oils, animal fat and waste cooking oils (WCOs). Soybean, palm and rapeseed are mainly used as biodiesel feedstock, as well as canola and sunflower. However, in recent years, the utilization of the edible oils has led to several food vs. fuel debates [4,5]. The cost of feedstocks from edible sources constitute around 70–80% of the final fuel production price, the cost of the feedstocks can be reduced by utilization of non-edible biodiesel feedstocks [6]. The Indian sub-continent has a potential to supply abundant non-edible feedstocks due to the vast forest regions and uncropped marginal and waste lands. Hence, India has high potential due to its endless supply of non-edible feedstocks, which makes it possible to overcome the economic challenges [7–10].

*Nigella sativa* (the black seed), which is found in the Middle East and Europe but is native to south-western Asia, it belongs to the plant family *Ranunculaceae*. B20 is the standard and acceptable form of running fuel in standard CI engines without engine modifications based on extensive literature about the use of biodiesel in diesel engines [11]. The authors, however, attempted to study the combined and symmetric effect of CRDI diesel engine characteristics of B25 and fuel additives. Several advantages of biodiesel are overcome by few disadvantages, such as damage to rubber hoses, higher production costs, fuel filter clogging, and fuel gelling due to high viscosity during cold weather. Hence, these factors have led to lower demand for biodiesel [6,12]. The drawbacks of biodiesel in diesel engine can be overcome by addition of a few milligrams of nanofuel additives [1,13,14]. Researchers in this field have investigated the effect of adding metallic and carbon-based nano-additives to diesel–biodiesel fuel blends; several have reported an overall improvement in the performance of the diesel engine and emissions reduction due to the complete combustion of fuel [1–3,15,16]

Due to their enhanced thermal and chemical properties and droplet combustion phenomena, asymmetric graphene oxide nanoparticles are more effective in reducing fuel emissions and improving performance than their metal-based counterparts, due to their enhanced thermal and chemical properties and droplet combustion behaviors and phenomenon [17]. The high exothermic heat release rate of graphene oxide NPs and the presence of oxygen functional groups, such as carboxylates, epoxides and hydroxides, promote chemically active spots resulting in overall fuel combustion [18]. The carbon depositions can also be addressed by addition of graphene oxide NPs, due to the presence of C, H and O atoms [19]. The majority of previous studies are based on the inclusion of metal-based nanoparticles

(such as aluminum oxide, zinc oxide, titanium oxide, cerium oxide, cobalt oxide, etc.) in the fuel blends. However, there is a lack of understanding about the combined effect of numerous high-energy-content carbon-based nanoparticles and alcohol additives in biodiesel blends. Hosseini et al. [20] investigated the effect on engine characteristics of carbon nanotubes (CNTs) (30, 60 and 90 ppm) and waste cooking oil (WCO-B5 and B10). The authors reported an increase of 8.21% in the BTE, whereas CO, HC, NOx and smoke emissions decreased by 65.7%, 44.98%, 27.49% and 29.41%, respectively. The specific fuel consumption (SFC) also decreased by 7.12%, while torque and power increased significantly with the addition of nanoparticles in WCO biodiesel. Aram Heidari M et al. [14] reported the addition of nano-additives of graphene quantum dot (GQD) in ethanol–biodiesel blends improved the performance and emission characteristics of a CI engine. The GQD in proportions of 30 ppm were added to ethanol–biodiesel (B10 and E2, E4, E6 and E8) blends. The engine speeds were varied at constant loads, and the authors reported an increase in power by 28.18% and torque by 12.42%. SFC, CO and HC decreased by 14.35%, 29.54% and 31.12%, respectively, in comparison with D100 fuel. Manzoore Elahi M Soudagar et al. [3] investigated the effect of graphene oxide nanoparticles on daily scum oil methyl ester (DSOME) using three nano-biodiesel fuel blends (DSOME (B20) + graphene oxide NP (ppm) dosage. The fuel blends used in the investigations were DSOME2020, DSOME2040 and DSOME2060; the nanofuel blend DSOME2040 (40 ppm of graphene oxide NPs in B20) illustrated overall enhancement in performance, combustion, and emission characteristics due to high catalytic activity of graphene oxide NPs. S. Abdul Sheriff et al. [11] investigated the combined effect of multi-walled carbon nanotubes (MWCNTs) and CeO2 in lemon and orange peel oil biodiesel fuel blends in CI engine. B20 + (50 and 100 ppm); eight different fuel blends resulted in reductions in BSFC, HC, CO and NOx emissions and increases in BTE at 100% load due to fine atomization of fuel particles, leading to complete combustion. Enhancement of the engine characteristics was also achieved by replacing the conventional fuel injector and combustion chamber. Pasupathy et al. [21] studied the simulation on the effect of piston bowl geometry on engine characteristics in a DI turbocharged CI engine for heavy duty applications using STAR-CD. The simulation results showed that the toroidal bowl's extended lip enhances the friction and thus increases the A: F mixture and decreases soot and specific fuel consumption. B.R. Ramesh Bapu et al. [22] investigated the effect of *Calophyllum inophyllum* biodiesel on a single-cylinder, VCR diesel engine. The modified HCC piston bowl geometry demonstrated reductions in the HC, CO and smoke emissions due to high turbulence and enhancement in the A:F mixture compared to conventional HCC. The modification of the piston bowl geometry led to an enhancement in the overall engine operations using the B20 fuel blend. Table 1 shows the symmetric effect of graphene nano-additives combined with diesel and biodiesel fuel blends on diesel engine performance and emission characteristics.

**Table 1.** The effect of graphene nano-additives mixed with diesel and biodiesel fuel blends performance and emission characteristics of diesel engines.

| Biofuel Blends | Biodiesel and GO NPs Size | Dosage of Graphene | Engine Type | Application Output | Ref. |
|---|---|---|---|---|---|
| D, B10, B20 and B20 nano-additive blends | *Ailanthus altissima*; 150 nm | 30, 60, and 90 ppm | 4-S Lombardini3LD510, SC, DI, CI engine, 1500 rpm, 18:1 CR. | • Reduction of BSFC, HRR and CP for B20G90<br>• Decrease in CO, NOx, smoke B20G90 and B10G90 | [23] |
| D, B20 and B20 nano-additive blends | *Jatropha*; 8 nm thick, 5 μm wide | 50 ppm<br>75 ppm | 4-S HATZ-1B30-2, SC, DI, CI engine, 1500 rpm 23°BDTC, AC, 21.5: 1 CR, 373 cm$^3$ displacement | • Improvement of calorific value, BTE and catalytic activity<br>• Better combustion and HRR, and enhanced air-fuel mixing<br>• Reduction of BSFC, NOx, CO, HC, smoke | [24] |
| D, B20 and B20 nano-additive blends | *Camelina* oil, Tree of heaven, Evening primrose; 150 nm | 60 ppm | 4-S Lombardini- 3LD510, SC, Non-TC, DI, CI 1500 rpm, engine, 18:1 CR | • Better atomization and rapid evaporation<br>• Reduction in BSFC, CO, HC and NOx.<br>• Increase in the oxidative stability | [25] |
| D and D nano-additive blends | GDD; 200 nm | 25 ppm | 4-S HATZ 1B30 light-duty, SC, DI, CI engine 3500 rpm, displacement 347 cm$^3$, NA, 21.5: 1 CR | • Decreases the BSFC<br>• Decreases CO, HC, NOx and ID.<br>• Higher in-cylinder temperatures and HRR | [26] |
| D, B20 and B20 nano-additive blends | Dairy scum oil; 23–27 nm | 20, 40 and 60 ppm | 4-S Kirloskar (TV1), SC, DI, CI engine, 2400 rpm, 23°BDTC, WC, 17.5: 1 CR, 3 FI nozzles | • Improvement of calorific value and HRR. Higher cetane number<br>• Enhancement of BTE, rapid ignition and fuel combustion<br>• Reduction in BSFC and average temperature of cylinder<br>• Increase in NOx emission<br>• Significant reductions in HC, CO and smoke emissions | [3] |
| D, B30 and B30 nano-additive blends | Palm; 23–26 nm | 50, 75 and 100 ppm | 4-S Kirloskar (TV1), SC, DI, CI engine, 2400 rpm, 0–25°BDTC, WC, 17.5: 1 CR, HCC | • High surface area of graphene oxide NPs increased the combustion characteristics.<br>• Increase in BTE and NOx emissions<br>• Reduction in BSFC, CO, HC, smoke | [27] |
| D, B20, B20 nano-additive blends | *Simarouba*, 22.5–26 nm | 20, 40 and 60 ppm | 4-S Kirloskar (TV1), SC, DI, CI engine, 1500 rpm, 23°BDTC, WC, 17.5: 1 CR, 3 FI nozzles | • Improvement of calorific value, BTE and HRR. Higher cetane number<br>• Reduction in BSFC and ID<br>• Increase in NOx emission<br>• Significant reductions in HC, CO and smoke emissions | [28] |

**Abbreviations:** D: Diesel, BD: Biodiesel, SC: Single Cylinder, TC: Twin cylinder, 4-S: Four Stroke, DI: Direct Injection, WC: Water-Cooled, AC: Air-Cooled, FI: Fuel Injector, CC: Combustion Chamber.

The current study is based on production of a much-less-explored, novel potential biodiesel feedstock, viz. *Nigella sativa*, and enhancement of the fuel properties of the *Nigella sativa* biodiesel through blending with graphene oxide nanoparticles and n-butanol fuel additives. The use of graphene oxide nanoparticles in *Nigella sativa* biodiesel improves the premixed combustion, resulting in a higher temperature in the combustion chamber. However, due to the high surface area of asymmetric graphene oxide nanoparticles, the thermal conductivity increases. In a single-cylinder common rail direct injection (CRDI) diesel engine with modified symmetric piston bowl geometry (Toroidal type) and a six-hole fuel injector, the effect of nanofuel blends are studied.

In this article, an attempt is made to study and analyze *Nigella sativa* methyl ester (NSME25) fuel properties with nanofuel and n-butanol blends (NSME25B10GO30, NSME25B10GO60, NSME25B10GO90 and NSME25B10GO120). A comparative analysis is carried out on the combined effect of NSME25 + n-butanol + graphene oxide fuel blends and NSME25 biodiesel fuel.

## 2. Materials and Methods

This section describes the production of *Nigella sativa* methyl ester using the transesterification reaction, characterization of graphene oxide nanoparticles, test engine setup and physicochemical properties of the test fuels.

### 2.1. Preparation of Nigella sativa Methyl Ester

*Nigella sativa* belongs to the botanical family *Ranunculaceae* and is generally referred to as black seed, black cumin seed, kalonji and seed of blessing, with an oil content of more than 35% [4,29]. It is generally used in traditional medicines like Unani and Ayurveda, *Nigella sativa* is mentioned in Tibb-e-Nabwi (Prophetic Medicine) for its usage on a daily basis for its ability to cure diabetes, renal and gastric-related diseases and use as a bronchodilator, anti-microbial treatment, etc. [30]. It is cultivated globally, but abundantly available in south and southwest Asia. The feedstock yields (85.6–97.7%) of biodiesel and can be deemed one of the key biodiesel feedstocks in Asia due to its high yield and availability [4]. The plant grows 20–90 cm tall and its leaves are finely segregated, with narrow linear treaded segments. The flowering petals are usually 5–10 in number and are symmetric, blue, white, pale pink and purple colored [31,32]. The seeds are dicotyledonous, regulose tubercular, tiny (2–3.5 mm/1–2 mm) and asymmetric, black on the outside and white on the inside, aromatic and bitter tasting [30]. Figure 1 shows the *Nigella sativa* plant, flowers, and seeds.
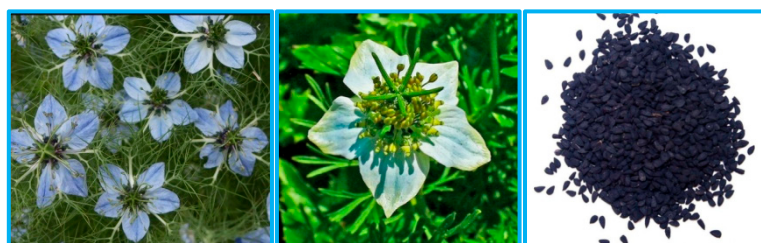


**Figure 1.** *Nigella sativa* plant, flowers, and seeds [32].

Crude *Nigella sativa* oil was purchased with a purity of 98.65% from local markets in India. The FFA% of the crude *Nigella sativa* oil is higher than the vegetable oils, hence transesterification reaction is employed in the current study. The method of transesterification was adopted from the previous investigation conducted on the production of *Nigella sativa* biodiesel [4,29]. Figure 2 illustrates the transesterification reaction of *Nigella sativa* oil.
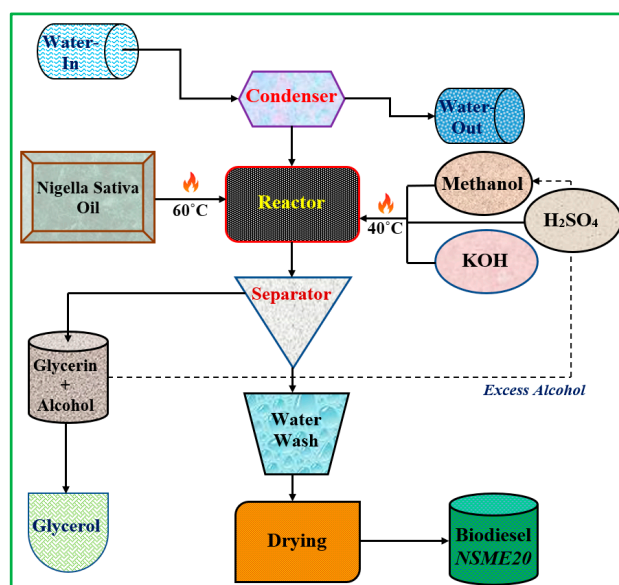
**Figure 2.** Transesterification reaction of *Nigella sativa* oil.

In the esterification process, the crude oil is initially mixed with methanol (CH$_3$OH- 2:1 volume) in a reactor at 60 °C for 3 h at steady stirring at a speed of 750 rpm. An application of 98% concentrated sulfuric acid (H$_2$SO$_4$: 1% vol/vol oil) is used to reduce the excess fat content of the esterified mixture. Additionally, 37% concentrated hydrochloric acid (HCl: 1% vol/vol oil) is used in the esterification reaction. The methanol and the esterified oil form an upper and lower layer, respectively. A separating funnel was used to separate the esterified oil from the methanol, then a rotary evaporator was used to remove the hints of moisture from the esterified oil. Further, the transesterification reaction (alkaline catalysis) was used in this investigation: the mixture of esterified oil and methanol (4:1) by volume of reactor was mixed with Potassium hydroxide (1%) and stirred at a constant speed of 750 rpm at 60 °C for two hours. Later, the biodiesel forms an upper layer in a separating funnel and a lower layer of glycerol. The obtained trans esterified oil was washed constantly using warm water, and the obtained biodiesel was stirred in a magnetic stirrer for removal of excess water, methanol, and moisture content. To finish, the biodiesel was washed with sodium sulphate (Na$_2$SO$_4$) and a fine meshed filter paper used to eliminate any traces of impurities. The conversion output of *Nigella sativa* methyl ester through the transesterification reaction is 92.8% weight. The biodiesel output was in symmetry with the preceding literature [2,3]. Table 2 illustrates the Fatty acid composition of *Nigella sativa* methyl ester.

**Table 2.** Fatty acid composition of *Nigella sativa* methyl ester.

| Fatty Acid | IUPAC Systematic Name | Carbon Content (C) | *Nigella Sativa* Biodiesel % Weight |
|---|---|---|---|
| Arachidic acid | Eicosanoic | 20:0 | 0.75 |
| Behenic acid | docosanoic acid | 22:0 | 1.8 |
| Erucic acid | cis-13-Docosenoic acid | 22:1 | 6.8 |
| Linoleic acid | cis-9-cis-12 Octadecadienoic | 18:2 | 45.66 |
| Linolenic acid | cis-9-cis-12 | 18:3 | 0.35 |
| Myristic acid | Tetradecanoic | 14:0 | 0.2 |
| Oleic acid | cis-9-Octadecenoic | 18:1 | 21.56 |
| Palmitic acid | Hexadecanoic | 16:0 | 15.65 |
| Stearic acid | Octadecanoic | 18:0 | 3.85 |

*2.2. Properties and Characterization of Graphene Oxide Nanoparticles*

The graphene oxide nanoparticles (GO) were prepared at lab scale in India; the method of preparation of graphene oxide nanoparticle additives is explained and is in symmetry with the

preceding research by Soudagar et al. [3]. The average size of the synthesized GO NPs was 23–27 nm (±0.5 nm). Figure 3 illustrates the XRD analysis of the graphene oxide nanoparticles.
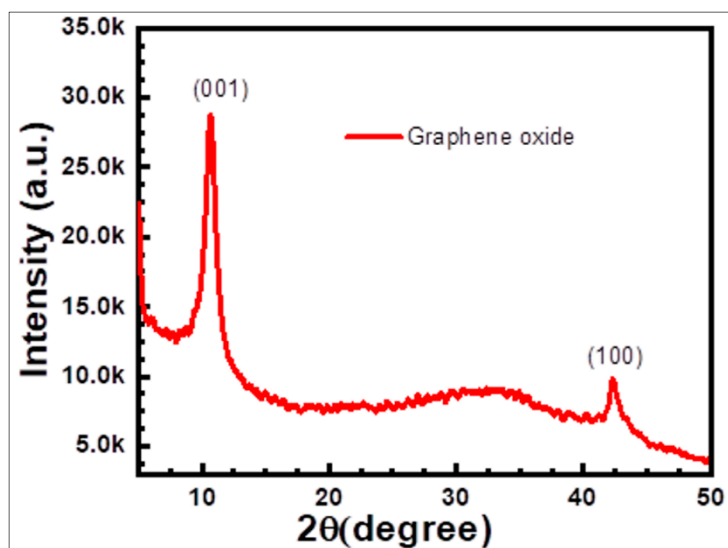


**Figure 3.** X-ray diffraction (XRD) spectra of graphene oxide.

The X-ray diffraction spectrum (XRD) was used to confirm a successful GO synthesis by identifying their cellular structural units (d-spacing). The analysis was carried out using a Bruker D8 ADVANCE diffractometer with radiation Cu K$\alpha$ ($\lambda$ = 1.54060 Å). Figure 3 illustrates the XRD patterns. The XRD pattern of asymmetric graphene oxide exhibits both a prominent peak of the (001) plane at 2$\theta$ = 10.74° and a (100) plane diffraction peak at 2$\theta$ = 42.34°, confirming the successful GO synthesis [33]. The SEM images shown in Figure 4a,b, the SEM and EDX were analyzed with EDAX using the Scanning Electron Microscope XL 30 ESEM. Resolution: up to 2; magnification: up to 250,000×, Acc. Voltage: 30 kV. It is evident that GO NPs have a multiple lamellar layer structure, and the edges of individual sheets can be distinguished from the SEM images. The asymmetric films are stacked above each other and display wrinkled areas. It can also be noted that the edges of the GO sheets were thicker. This is because the functional groups containing oxygen were mainly combined at graphene oxides edges. From the EDX analysis in Figure 4c, it is evident that the GO contains around 61.13% at. C, 38.65% at. % O and 0.23% atom S. Hence, the graphene oxide contains sufficient carbon and oxygen which confirms successful synthesis of GO nanoparticles.

The TEM images are also illustrated in Figure 4d, 50 nm and Figure 4e, 200 nm; Figure 4f illustrates the Selected area (electron) diffraction (SAED) pattern; Figure 4g shows the High-resolution transmission electron microscopy (HRTEM) pattern. The TEM and HRTEM study was performed using JEOL 2000 FX-II TEM with an ultra-thin Oxford Instruments EDS window system. The appearance of TEM images of GO NPs are multilayered and wrinkled. The HRTEM demonstrates the lattice fringes of graphene oxide nanoparticles [34,35]. The crystallographic structure of the graphene oxide was characterized by the SAED pattern. The previous research cited illustrates a single set of hexagonal diffraction patterns with sharp, symmetric and clear diffraction spots in the graphene oxide nanoparticles [35].
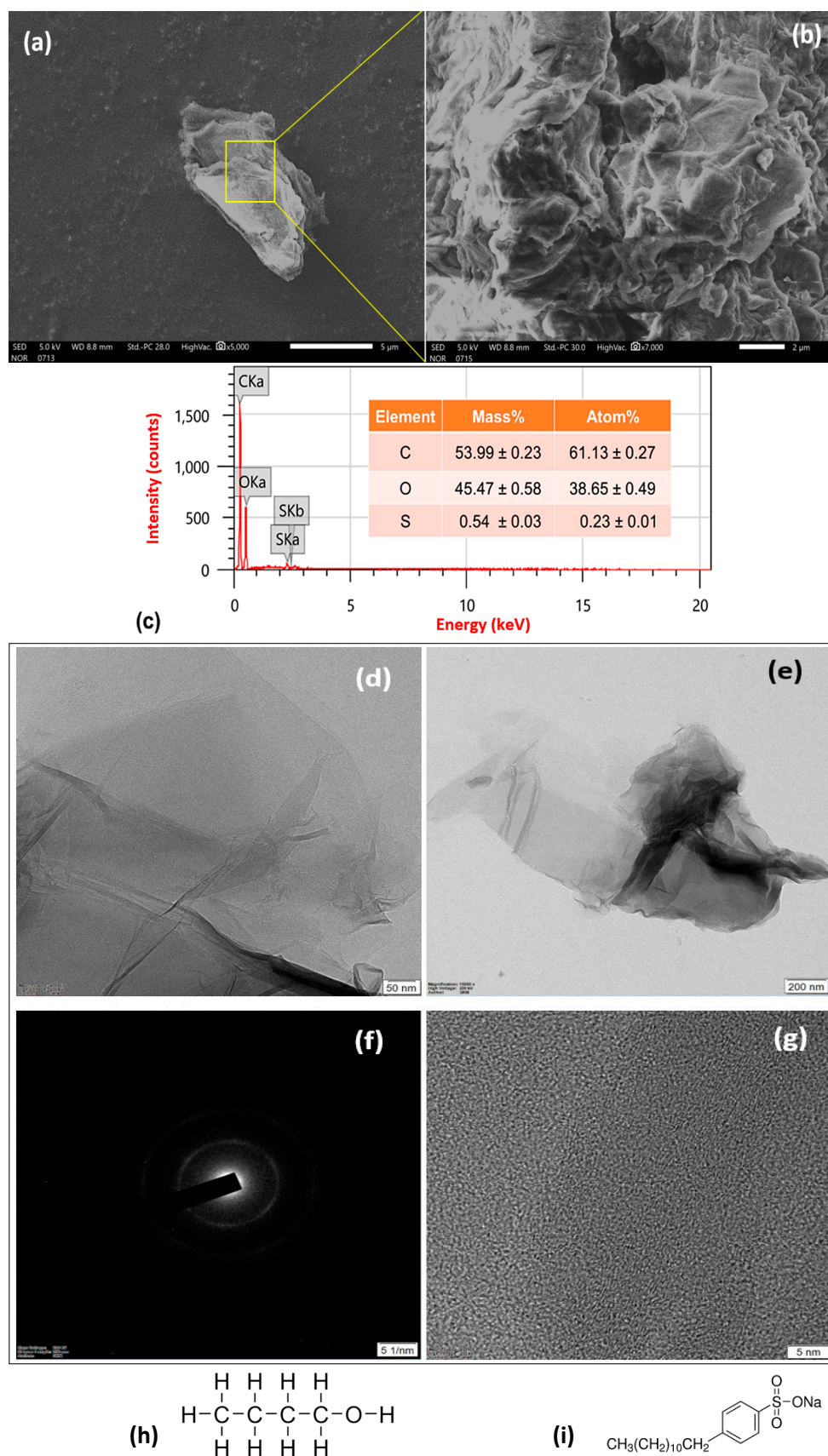
**Figure 4.** SEM images of GO: (**a**) 5 μm; (**b**) 2 μm; (**c**) EDX analysis; TEM images (**d**) 50 nm and (**e**) 200 nm; (**f**) SAED pattern; (**g**) HRTEM pattern; (**h**) Chemical structure of n-butanol; (**i**) Chemical structure of SDBS surfactant.

n-butyl alcohol or butanol is a primary alcohol consisting of a four-carbon chain structure and the chemical formula is $C_4H_9OH$. Its isomers of n-Butanol include tert-butanol, 2-butanol, and iso-butanol. Figures 4h,i illustrates the chemical structure of n-butanol and SDBS surfactant. Butanol belongs to the group of fusel alcohols in German language or bad liquor and is readily soluble in water. Fermentation of sugars and carbohydrates produces n-Butanol, and it is also found in several food products and beverages [36,37]. Butanol is essentially a petrochemical substance and is made from propylene. n-butanol is used as a diesel and gasoline substitute. Butanol is also known for its use as a biofuel; 85 percent of butanol can be used in diesel and petrol-powered cars without engine modification, providing more energy than ethanol [38]. To reduce the soot emissions, butanol is added to diesel fuel [39]. In the current investigation, commercially available n-butanol and SDBS surfactant were procured from Sigma Aldrich. The addition of surfactant enhances the stability of NPs in aqueous suspensions to convert the surfaces of NPs from hydrophobic to hydrophilic and conversely to non-aqueous. It also reduces the possibility of surface tension, coagulation and coalescence and breaks the asymmetric bonds. They tend to position themselves and establish a degree of continuity between the NPs and the base fluid at the interface [1].

*2.3. Test Engine Setup*

In the current investigation, Kirloskar TV1 was assisted by a common rail direct injection system, four-stroke, water-cooled diesel engine. In the current world scenario, the fuel efficiency of diesel engines is increased by the application of CRDI; nowadays, CRDI technology is widely used in commercial vehicles [40]. In order to increase the fuel injection pressure to 900 bar, the regulatory pressure valve and the fuel injector are attached to the existing engine. The schematic representation of the CRDI engine test rig is illustrated in Figure 5. The engine runs at a constant speed of 1500 rpm; the CRDI engine's rated power output is 5.2 KW; it has a 900 bar injection pressure and 23° BTDC injection timing. Several temperatures (water inlet and outlet temperature, exhaust gas temperature) were measured using thermocouples. The combustion chamber used in the current investigation is a toroidal type, replacing the hemispherical combustion chamber for better mixing of the A:F. A solenoid six-hole, 0.1-mm orifice diameter fuel injector at 900 bar injection pressure is used. Figure 6 illustrates the top and side views of the Toroidal combustion chamber (TCC) used in the current investigation.
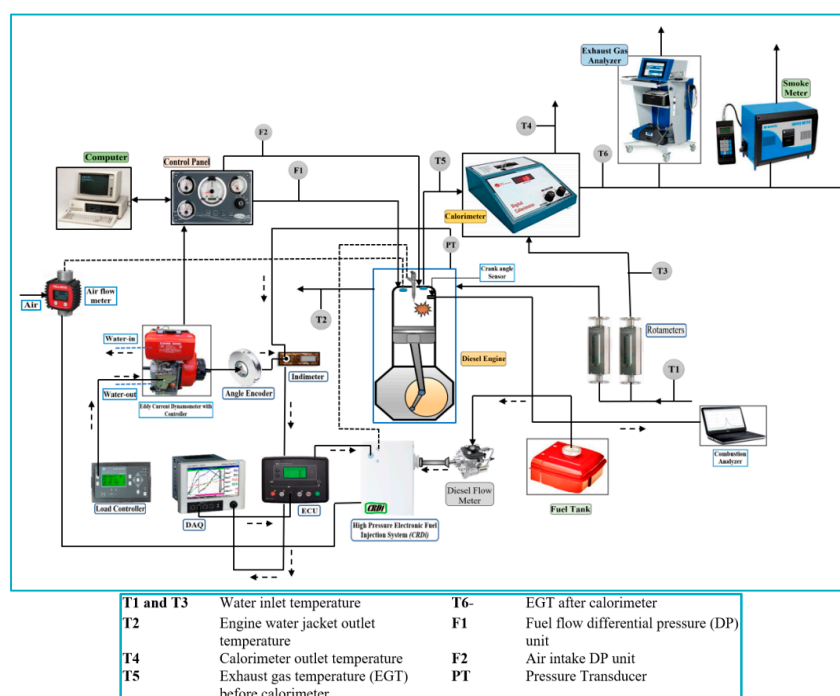


| T1 and T3 | Water inlet temperature | T6- | EGT after calorimeter |
| T2 | Engine water jacket outlet temperature | F1 | Fuel flow differential pressure (DP) unit |
| T4 | Calorimeter outlet temperature | F2 | Air intake DP unit |
| T5 | Exhaust gas temperature (EGT) before calorimeter | PT | Pressure Transducer |

**Figure 5.** Schematic line diagram of common rail direct injection diesel engine setup.

**Figure 6.** Top and side views of the Toroidal combustion chamber.

*2.4. Preparation of Fuel Blend*

In the current investigation, a two-step process for the preparation of nanofluids is used; the graphene oxide nanoparticles are steadily dispersed in the SDBS surfactant and distilled water using a probe sonicator, which is also known as the indirect mode of sonication.

The oxygenated additive, n-butanol, is blended with biodiesel at a constant volume of 10% during the ultasonication process of NPs and fuel. The fuel blends are dosed with graphene oxide nanoparticles at 30, 60, 90 and 120 mg/L dosage levels using a magnetic stirrer for 25 min, 1 h using an ultrasonicator bath and 20 min using a probe sonicator at a frequency of 15–20 Hz per three seconds. Table 3 illustrates the composition of test fuel blends.

The fuel blend NSME25B10GO30 is prepared by blending NSME25 with 30 ppm graphene oxide NPs and 15 ppm of SDBS surfactant. For the NSME25B10GO60 blend, NSME25 is blended with 60 ppm graphene oxide NPs and 25 ppm SDBS surfactant. For NSME25B10GO90 and NSME25B10GO120 fuel, NSME25 biodiesel is blended with 90 ppm and 120 ppm of graphene oxide NPs and 35 ppm and 45 ppm of SDBS surfactant, respectively. For preparation of nanofluids, the ultrasonic waves are supplied to a combination of distilled water (5 mL), graphene nanoparticles and SDBS surfactant using a probe sonicator at a frequency of 20 KHz for 20–30 min for each nanofluid blend. The sonication breaks the intermolecular and symmetric interactions which prevents the agglomeration. Later, the NSME25 biodiesel is blended with the nanofluids, the blend is stirred using a magnetic stirrer at 60 °C to remove the water and moisture content for 15 min, a bath-type sonicator is used for blending the different sets of nanofuel blends for one hour for each blend, and, further, the nanoparticle stability is increased by sonicating in a probe sonicator. These steps ensure synthesis of stable nanofuel blends. Figure 7 shows the steps and methodology adopted in the study on nanofuel blends.
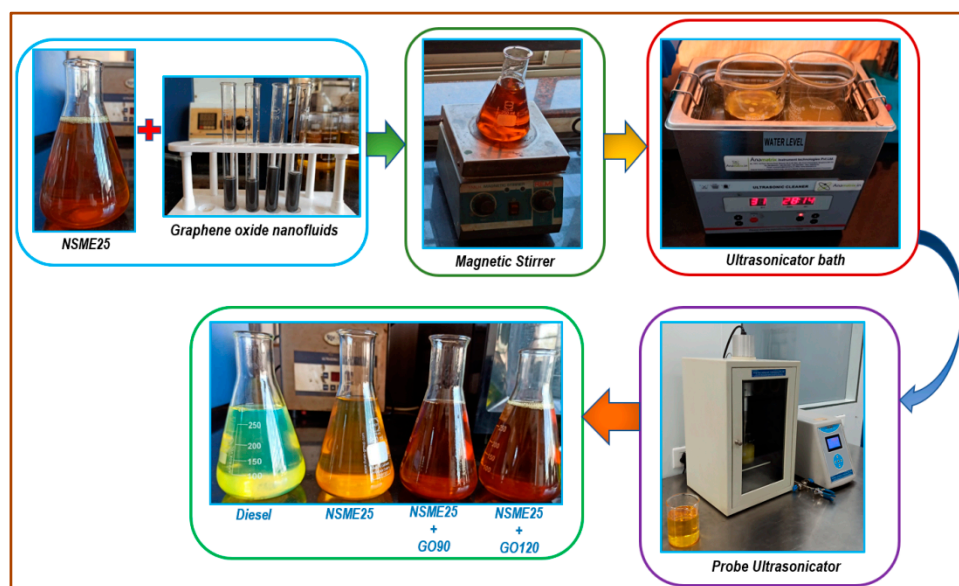


**Figure 7.** Methodology adopted in the study on nanofuel blends.

**Table 3.** Composition of test fuel blends.

| Fuel Blend | Diesel | Diesel qty. | Biodiesel | Biodiesel Qty. | n-butanol | n-butanol Dosage | GO NPs Dosage | SDBS Surfactant |
|---|---|---|---|---|---|---|---|---|
| Diesel | 100% | 1000 mL | - | - | - | - | - | - |
| NSME25 | 75% | 750 mL | 25% | 250 mL | - | - | - | - |
| NSME25B10GO30 | 65% | 650 mL | 25% | 250 mL | 10% | 100 mL | 30 ppm | 15 mg |
| NSME25B10GO60 | 65% | 650 mL | 25% | 250 mL | 10% | 100 mL | 60 ppm | 25 mg |
| NSME25B10GO90 | 65% | 650 mL | 25% | 250 mL | 10% | 100 mL | 90 ppm | 35 mg |
| NSME25B10GO120 | 65% | 650 mL | 25% | 250 mL | 10% | 100 mL | 120 ppm | 45 mg |

*2.5. Physicochemical Properties of Fuel Blends*

The prepared fuel blends are compared with diesel and *Nigella sativa* biodiesel using ASTM D6751-15c standards. NSME25 fuel blend's calorific value is the lowest amongst all the fuel blends, and also showed the highest density and viscosity. The addition of n-butanol to the *Nigella sativa* biodiesel showed higher miscibility and stability rates. Furthermore, the addition of n-butanol and graphene oxide NPs to the fuel samples reduces the ID period due to enhancement of the combustion phenomenon and reductions in the combustion duration, density, viscosity, and emissions. Table 4 demonstrates the physicochemical properties of fuel blends in accordance with the ASTM standards.

The overall cost for experimentation and synthesis of nano-fuel blends, which includes the engine operating cost, transportation, electricity, and labor, was around $210.64 (₹ 15,771.88, conversion from USD to INR, April, 2020). The use of nanoparticles in the biodiesel fuel marginally raises the fuel cost by around 2.56%. Nevertheless, graphene oxide nano-additives and n-butanol increase the overall fuel characteristics, which overcomes the cost setting.

**Table 4.** Physiochemical properties of diesel, *Nigella sativa* methyl ester and nanofuel blends.

| Properties | Unit | ASTM Standards (D6751-15c) | Test Limit | Diesel [a] | NSME25 [a] | NSME25 B10GO30 [a] | NSME25 B10GO60 [a] | NSME25 B10GO90 [a] | NSME25 B10GO120 [a] |
|---|---|---|---|---|---|---|---|---|---|
| Kinematic Viscosity | cSt at 40 °C | ASTMD445 | 1.9–4.1 | 2.35 | 4.812 | 3.256 | 3.395 | 3.412 | 3.564 |
| Calorific value | MJ/kg | ASTM D5865 | Min. 35,000 | 45.456 | 41.25 | 42.105 | 42.759 | 43.58 | 43.017 |
| Density | kg/m$^3$ at 15 °C | ASTM D4052 | 820–840 | 822.68 | 877.61 | 860.5 | 856.45 | 850.41 | 852.6 |
| Specific Gravity | gm/cc | ASTM D891 | 0.87–0.90 | 0.8 | 0.862 | 0.856 | 0.855 | 0.854 | 0.8548 |
| Flash Point | °C | ASTMD93 | Min. 93 | 78 | 130.55 | 120.86 | 118.45 | 110.68 | 112.81 |
| Pour Point | °C | ASTM D97-12 | −15 to 16 | −4 | 3.2 | 2.52 | 2.18 | 2.02 | 2.1 |
| Cloud point | °C | ASTM D2500-11 | −3 to 12 | −1 | 5 | 5.47 | 5.43 | 5.42 | 5.423 |
| Cetane Number | - | ASTMD613 | Min. 40 | 49.52 | 45.68 | 50.63 | 50.85 | 51.27 | 51.91 |

[a] Analysis result.

## 3. Uncertainty Analysis of Expected Errors

Uncertainty analysis is the systematic and symmetric set of procedures followed for calculation of errors in experimental data. The inaccuracies occur due to the error in electronic and mechanical components, environmental factors, and human miscalculations [41,42]. The information is gathered at standard conditions, and the specifications and details of all the components are already available. Measurement errors which come from several different sources are classified into bias and precision errors; throughout the experimentation, the bias errors remain constant. The measurement uncertainty is estimated as the experiments are carried out. The uncertainty measurements using standard parameters are explained in this section.

The propagation of uncertainty for parameters that have been determined on the factors depending on two or more independent parameters is determined using Equation (1),

$$\frac{U_y}{y} = \sqrt{\left(\frac{u_{x_1}}{x_1}\right)^2 + \left(\frac{u_{x_2}}{x_2}\right)^2 + \ldots\ldots\ldots\ldots + \left(\frac{u_{x_n}}{x_n}\right)^n} \tag{1}$$

where, $U_y$ is uncertainty; $y$ is testing value; $x_1, x_2, \ldots, x_n$ are evaluated parameters, and the uncertainty of emissions is $U_y = \frac{Resolution}{Range}$.

The overall uncertainty of the parameters of engine performance, emission, and combustion is calculated using Equation (2). Table 5 also illustrates the uncertainty and accuracy levels of calculated engine parameters.

$$
\begin{aligned}
&\text{Overall uncertainty} = \\
&\pm \sqrt{Uncertainty \% \ of \ (BTE^2 + BSFC^2 + CO^2 + NOx^2 + HC^2 + smoke^2 + HRR^2 + EGT^2)} \\
&= \sqrt{Uncertainty \% \ of \ (0.5^2 + 0.4^2 + 0.35^2 + 0.4^2 + 0.4^2 + 0.35^2 + 0.18^2 + 0.5^2)} \\
&= \pm 1.12
\end{aligned} \tag{2}
$$

The overall uncertainty for the measured parameters is ±1.12, which is within the permissible limit and in symmetry with previously reported studies [2,3].

**Table 5.** Uncertainty and accuracy levels of calculated engine parameters.

| Parameters | Accuracy (±) | Uncertainty (%) |
|---|---|---|
| CO emission (%) | ±0.01% | ±0.35 |
| NOx emission (ppm) | ±10 ppm | ±0.4 |
| HC emission (ppm) | ±10 ppm | ±0.4 |
| Exhaust gas temperature (°C) | ±1 | ±0.5 |
| Smoke meter (HSU) | ±1 | ±0.35 |
| Brake Thermal Efficiency (%) | - | ±0.5 |
| Brake Specific Fuel Consumption (%) | - | ±0.4 |
| Heat Release Rate (J/°CA) | - | ±0.18 |

## 4. Results

### 4.1. The Effect of Graphene Oxide Nanoparticles and n-Butanol in Biodiesel Nigella sativa on the Combustion Characteristics of CRDI Engines

#### 4.1.1. The Effect of Fuel Additives on Heat Release Rate

The HRR is negative during the ID period due to the cooling effect produced by the vaporization of the fuel and the loss of heat at the cylinder walls. The increase in HRR for all nanofuel mixtures is due to an improved cetane number and a lower ID period, which helps in increasing the engine efficiency [42–45]. Figure 8 shows the variation of HRR and crank angle for test fuels at maximum load.
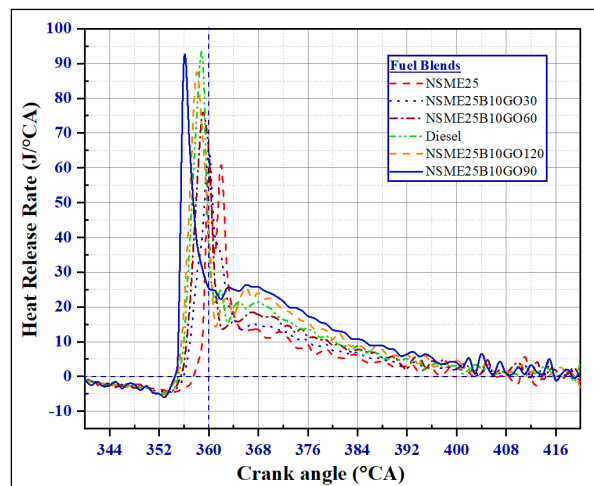
**Figure 8.** The variation of HRR and crank angle for test fuels at 100% load.

Owing to higher molecular weight and lower burning velocity, the HRR for the NSME25 blend is lower than the other fuel blends [46]. The enhancement in HRR for the all nanofuel blends is due to improved surface-area-to-volume ratio, high ignition and improved fuel properties and thermal conductivity [47,48]. This results in an increase in the peak pressure and, hence, the HRR is also increased. The maximum peaks observed for NSME25B10 GO (30, 60, 90 and 120 mg/L) were 65.25, 75.72, 90.54 and 87.223 J/°CA, while the peaks observed for diesel and NSME25 were 91.997 and 60.813 J/°CA. An enhancement of 29.727 J/°CA in HRR was observed with the addition of 90 ppm of GO and 10% volume n-butanol to NSME25 when compared with neat NSME25.

## 4.1.2. Effect of Fuel Additives on the In-Cylinder Temperature of the Engine

The mean value of cylinder temperature of combusted and unburned gases in the combustion chamber that occurs during a cycle is known as in-cylinder or mean cylinder temperature. The gases in the cylinder are a symmetric blend of combusted and unburned air and fuel. The temperature in the cylinder determines the fuel's combustion reaction rate, and the desired value should be closer to the adiabatic flame temperature ($T_a$) [49]. Figure 9 demonstrates the variation of heat release rate and crank angle for test fuels at maximum load.
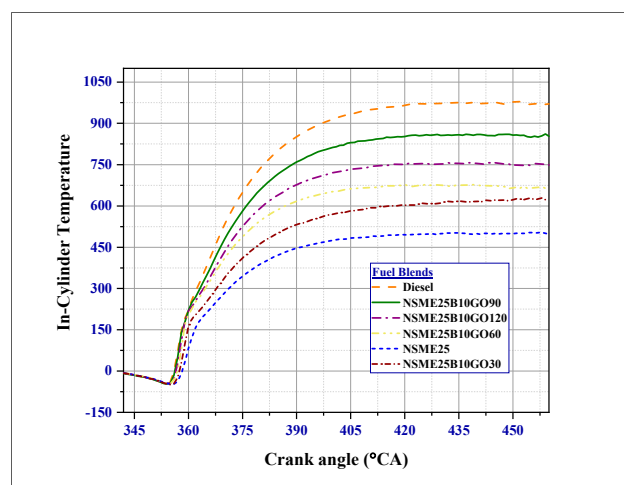


**Figure 9.** The variation of heat release rate and crank angle for test fuels at 100% load.

The adiabatic temperature is achieved when there is no loss in thermal energy and the adiabatic state is reached. It is observed that there is a 15° ATDC distance in the injector where flame reaches the

wall of the cylinder [49,50]. At this point, maximum pressure is reached, although the combustion process is incomplete and the combustion at the boundary of the combustion chamber continues a further few °CA [50]. Initially, the CRDI engine was operated on diesel fuel; diesel showed a maximum in-cylinder temperature of 973.51 °C to 970.963 °C from 422 °CA to 460 °CA. The nanofuel blend, NSME25B10GO90, illustrated a mean cylinder temperature of 851.63 °C to 852.94 °C at 418 °CA to 460 °CA. Meanwhile, the mean cylinder temperature of all the nanofuel mixes at dosage levels of 30, 60 and 120 mg/L showed an increase in the temperature of the in cylinder. Due to high viscosity and density, NSME25 however reduced the mean cylinder temperature.

### 4.1.3. The Effect of Fuel Additives on Exhaust Gas Temperature (EGT)

The variation of the exhaust gas temperature (EGT) and engine brake power is shown in Figure 10 for different fuel blends. An increasing trend in EGT was observed for increasing loads. Lowest EGT (395 °C) was observed for diesel fuel and highest EGT (480 °C) was observed for Nigella biodiesel at maximum load; 90 ppm of graphene oxide NPs with 10% n-butanol additive illustrated a very close range of values of EGT with diesel at all brake powers, the EGT at maximum load is (413 °C). Nigella biodiesel combined with n-butanol 10% and 30 ppm of graphene illustrated slightly lower EGT compared with NSME25.

This indicates the reduction in EGT with the presence of nano-additives. The GO nanoparticles have higher thermal conductivity than the NSME25, which helps in faster heat transfer. The biodiesel blends exhibits improper combustion in the engine due to their viscous nature and lower calorific value. This leads to an increase in heat in the combustion chamber due to many unburnt gases during the process of the combustion phenomenon and temperature rise. Lower concentrations of graphene oxide nanoparticles showed higher EGT, while higher content of nanoparticles reduced the EGT.
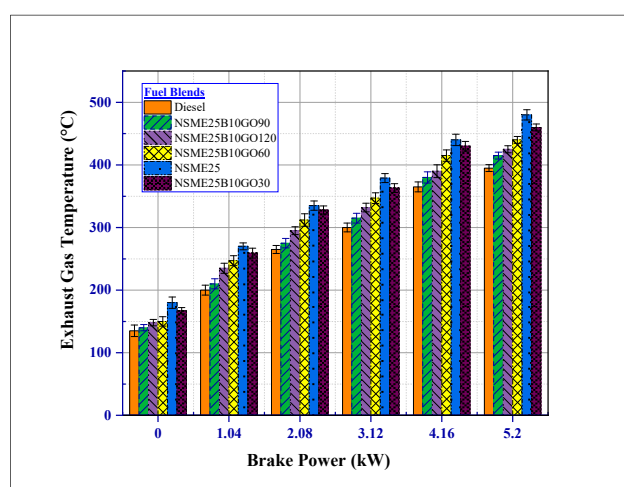


**Figure 10.** Variation in exhaust gas temperature and crank angle at maximum load for all test fuels.

### 4.1.4. The Effect of Fuel Additives on Cylinder Pressure (CP)

The burnt fuel fraction determines the peak cylinder pressure in a diesel engine during the initial combustion time (pre-mixed stage of burning). The CP is a function of the crank angle from the end of the compression stroke and in the early portion of the power stroke. The amount of fuel burnt during the uncontrolled combustion process is directly related to the engine cylinder pressure production.

Figure 11 shows the variation in the crank angle of the cylinder pressure at full load. The addition of GO NPs and n-butanol to *Nigella sativa* biodiesel leads to production of higher oxygen and improves the cetane content, and the large volume-to-asymmetric-surface-area ratio result in an increase in the cylinder pressure. The NSME25 illustrated the lowest CP due to high viscosity; however, addition of

90 mg/L of GO NPs and 10% n-butanol increased the CP. A reasonable increase was observed for all the nanofuel blends when compared with NSME25.
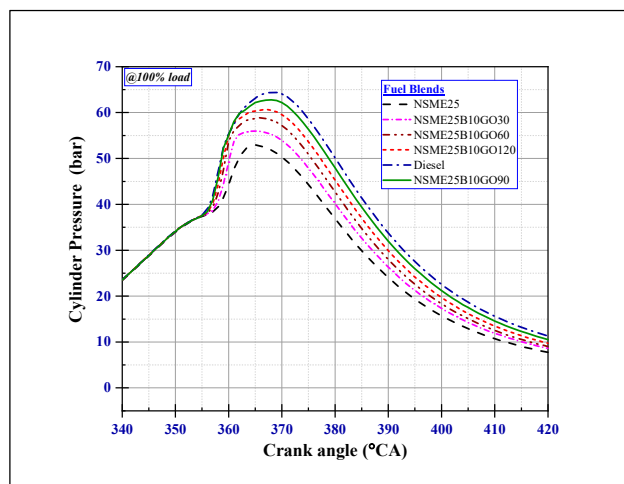


**Figure 11.** Variation of cylinder pressure and crank angle with maximum load for all test fuels.

### 4.1.5. The Effect of Fuel Additives on Ignition Delay (ID) Period

The ID occurs in the combustion chamber mainly due two attributes, the chemical and the physical delay. The chemical delay is due to pre-combustion reactions in the mixture of fuel and air. The physical delay is due to the vaporization, atomization and mixing of the fuel–air mixture [48]. Figure 12 shows a declining trend in the ignition delay period with an increase in brake power. The chamber combustion temperature rises with brake power, resulting in physical delay attributed to ignition delay. Additionally, the ignition delay is reduced, due to lower fuel viscosity, density and bulk modulus [51].
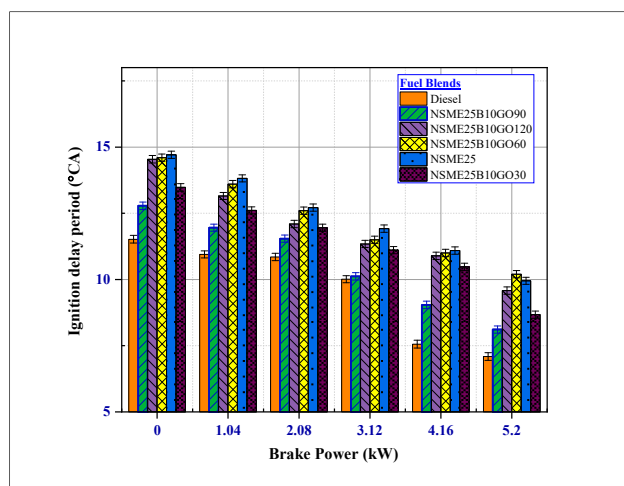


**Figure 12.** Variation of ignition delay period and brake power for test fuels at maximum load.

Nigella biodiesel (NSME25) illustrated poor fuel properties; hence, the delay is maximum, while 90 ppm of GO NPs with 10% n-butanol additive mixed with biodiesel has closer values to diesel due to better combustion characteristics. NSME25B10GO90 exhibited 8.11 °CA compared with NSME25 ID (10.2 °CA); the increase in the ID period for NMSE25 might be due to higher viscosity rate. The ignition delay reduces the brake power of all mixtures due to the higher engine temperature, which causes faster and symmetric combustion of fuel. [15]. Additionally, the reduction in the ID is due to enhanced A:F mixing, which results in an improved combustion due to secondary atomization and

micro-explosion. The ID decreases with an increase in the load; a difference of 4.45 °CA is observed for diesel fuel from minimum to maximum loading conditions. Additionally, the ID period of diesel and NSME25B10GO90 fuel blends was comparable at all the load conditions.

### 4.2. The Effect of Graphene Oxide Nanoparticle and n-Butanol in Nigella sativa Biodiesel on the CRDI Engine Performance Characteristics

#### 4.2.1. The Effect of Fuel Additives on Brake Thermal Efficiency (BTE)

BTE is the BP (Brake Power) of an engine as an application of thermal energy input from the fuel; it is the measure of the conversation of heat energy from fuel to mechanical power.

Figure 13 shows the variance of BTE with BP at constant load; the results showed that the CRDI diesel engine's BTE increased at all graphene oxide NP dosage levels. Compared with the neat diese—biodiesel fuel blends, the oxides of carbon-based nanoparticles facilitate complete combustion of the fuel charge. Graphene oxide serves as an oxygen buffer and thus increases the BTE [24]. As the dosage of graphene NPs in the fuel blends increases, the BTE increases. An increase of 18.37 % was observed in the BTE with the addition of 90 ppm of GO NPs and 10% n-butanol additives in *Nigella sativa* biodiesel at maximum load compared to the neat NSME25. However, the BTE decreases significantly at higher concentrations of asymmetric GO NPs (120 ppm), leading to an increase in viscosity and density of the fuel blend. The BTE values for the NSME25B10GO90 nanofuel blends were also comparable with diesel. The increase in BTE for all the nanofuel mixtures at specific loads is due to the enhanced symmetric micro-explosion phenomenon and higher catalytic activity of NSME25 GO NPs [24].
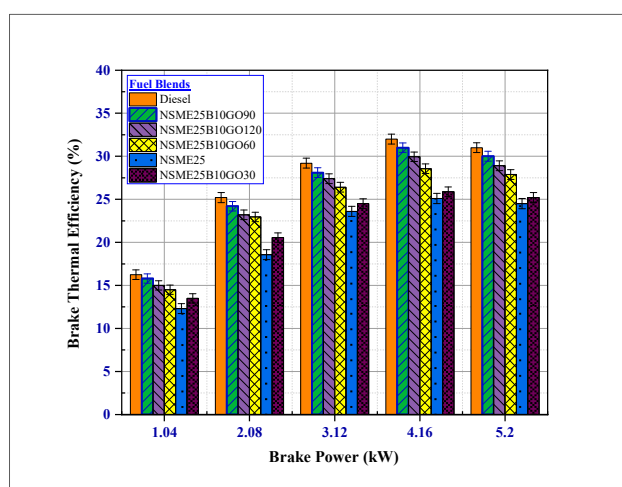


**Figure 13.** The variation of BTE and load at different BP for fuel blends.

#### 4.2.2. The Effect of Additives on Brake-Specific Fuel Consumption (BSFC)

BSFC is a diesel engine's efficiency to completely combust the fuel charge and generate shaft power. This is the ratio of the fuel consumed to the power generated. The ignition delay is highly dependent on the cetane number of the fuel blend, which determines the duration of the lag. Therefore, cetane number is a critical diesel fuel property which has a major impact on the CD. The atomization of fuel is also inversely proportional to the kinematic viscosity and density of [52].

Figure 14 shows the variation of BSFC and loads for fuel blends at different BP. NSME25 fuel blends' high viscosity and density decrease the fuel atomization process; thus, adding n-butanol to the fuel decreases density and viscosity and increases the calorific value and cetane number of the fuel blends by supplying more oxygen for complete combustion, resulting in a high degree of vaporization [53–57]. The high catalytic activity and high reactive surface area of the GO NPs also enhances the micro-explosion phenomenon [25]. Hence, the addition of additives to *Nigella sativa*

biodiesel enhances the fuel combustion process, resulting in complete combustion, which reduces the fuel consumption. The BSFCs observed for the NSME25B10 GO (30, 60, 90 and 120 ppm) were 325, 310, 260 and 285 g/kWh, respectively, compared to 345 g/kWh for NSME25 and 248 g/kWh for D100 at maximum load.
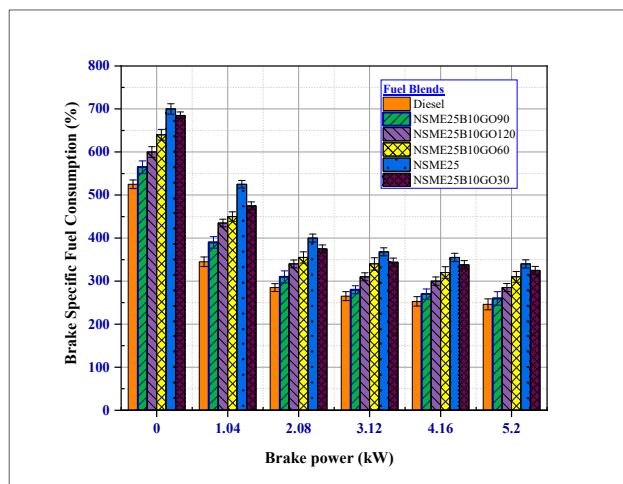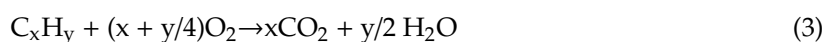


**Figure 14.** The variation of BSFC and load at different BP for fuel blends.

*4.3. The Effect of Graphene Oxide Nanoparticle and n-Butanol in Nigella sativa Biodiesel on the Emissions of the CRDI Engine*

The general equation for combustion of hydrocarbons is represented by Equation (3).

$$C_xH_y + (x + y/4)O_2 \rightarrow xCO_2 + y/2\ H_2O \qquad (3)$$

The carbon (C) and hydrogen (H) atoms react to form $CO_2$ and $H_2O$; a lack of oxygen molecules during fuel combustion leads to incomplete combustion. The exhaust gas content after the combustion process is described in Figure 15.
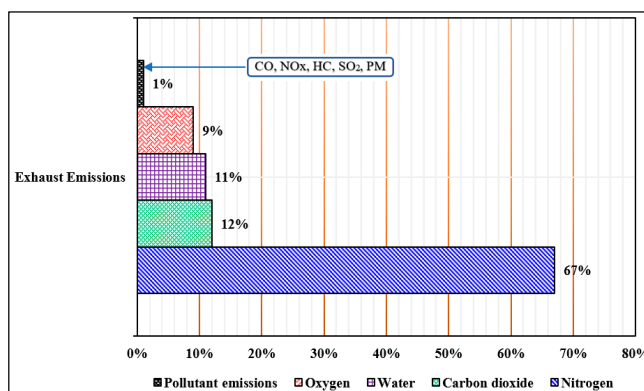


**Figure 15.** The composition of exhaust emissions from an automobile [58]

4.3.1. The Effect of Fuel Additives on Carbon Monoxide (CO) Emissions

The incomplete combustion of fuel charge in the combustion chamber, with partial and asymmetric oxidation, contributes to carbon monoxide emissions. CO is produced during instantaneous acceleration and the engine starting phase, where there is necessity of a rich A:F mixtures. Hence, hydrocarbons, due to a shortage of oxygen molecules, convert the carbon dioxide to carbon monoxide. Figure 16 illustrates the variation of CO emissions and BP for test fuels.
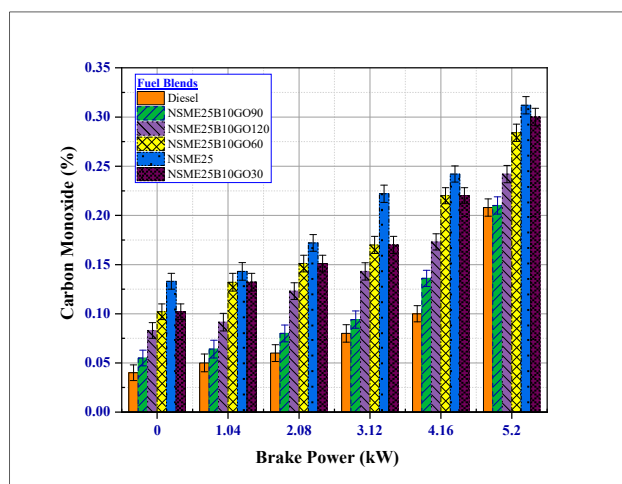
**Figure 16.** Variation of CO emissions and BP for test fuels.

The diesel fuel showed the lowest CO emissions, due to low viscosity, high calorific value and high heat release rate, which led to complete fuel combustion [23,59]. Meanwhile, NSME25 illustrated the highest CO emissions at all loads, owing to the rich A:F mixture, shortage of oxygen atoms in the combustion chamber, high density and viscosity and poor rate of combustion. The extra oxygen atoms in the combustion chamber are supplied through the addition of butanol, which acts as an oxygenated additive, and, for rapid combustion [57], the calorific value of the fuel is increased through addition of asymmetric graphene oxide nanoparticles. The graphene oxide and butanol improve the combustion characteristics of NSME25, by enhancing the oxidation, combustion rate, and calorific value and sustaining a desired combustion chamber temperature. The NSME25B10 + GO (90, 120, 60 and 30) reduced the CO emissions by 50.15%, 29.925%, 9.84% and 4.56% compared to NSME25. Additionally, the CO emissions for 90 ppm of GO in NSME25 were comparable to diesel fuel at all loads. Hence, the addition of GO NPs and n-butanol fulfils the deficient oxygen atoms, which convert the CO emissions to $CO_2$, therefore precluding the toxic emissions [1,3,7,54].

4.3.2. The Effect of Fuel Additives on Hydrocarbon (HC) Emissions

The activation energy in the graphene oxide NPs in the fuel blends combusts the carbon particles within the combustion chamber at cylinder wall temperature, minimizing HC emissions for all nanofuel blends [51,60]. Figure 17 illustrates the variation of hydrocarbon emissions and brake power for test fuel blends.
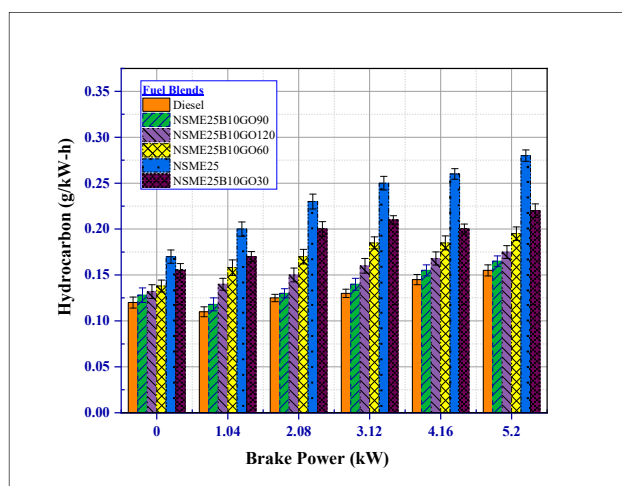


**Figure 17.** Variation of hydrocarbon emissions and brake power for test fuel blends.

The mixture of *Nigella sativa* biodiesel, 10% butanol and different dosage levels of GO NPs illustrated an overall reduction in the HC emissions compared to *Nigella sativa* methyl ester (NSME25). The fuel blend NSME25B10GO90 showed the lowest HC emissions compared 30, 60 and 120 ppm of GO NPs. The HC emissions observed for 90 ppm at of GO NPs and 10% butanol at maximum load were 0.0058 g/kWh; the emission was also 0.0002 g/kWh less than neat diesel and 0.2742 g/kWh lower than NSME25; the reduction in HC emission for NSME25B10GO90 fuel blend was around 3.44% and 48.72% less than diesel and NSME25, respectively. This is due to high surface catalytic activity inside the combustion chamber, resulting in acceleration of the combustion of asymmetric fuel particles with air [3,48,60].

### 4.3.3. The Effect of Fuel Additives on Nitrogen Oxide (NOx) Emissions

The temperature of oxygen and its concentration in the combustion chamber are the major contributors to NOx formation [1,61,62]. The variation of NOx emissions and brake power for test fuel blends is shown in Figure 18.
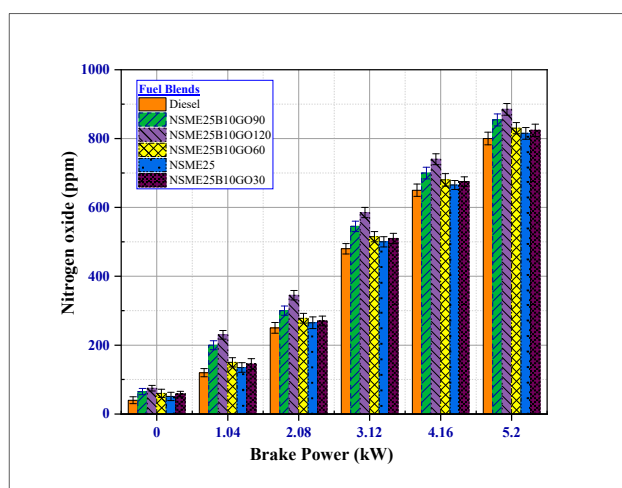


**Figure 18.** Variation of NOx emissions and brake power for test fuel blends.

NOx emissions from NSME25 and NSME25B10 (GO-30, 60, 90 and 120 ppm) are higher than from diesel. The possibility of high NOx emissions is due to the presence of excess oxygen molecules, the oxygen buffering additive, 10% butanol and the various dosage levels of GO NPs, which supply more oxygen atoms. Other explanations are the probable increase in the peak cylinder pressure, which results in high NOx emissions. The nanofuel blend NSME25B10GO120 emits the highest NOx emissions due to high percentage of oxygen-donating GO NPs and the presence of butanol; the emissions for NSME25B10GO (120 and 90) are 885 ppm and 854 ppm, while diesel and NSME25 emitted 800 ppm and 815 ppm, respectively.

### 4.3.4. Effects of Fuel Additives on Carbon Dioxide ($CO_2$) Emissions

Compared to the B20 fuel blend, the addition of graphene oxide nanoparticles to *Nigella sativa* biodiesel reduces $CO_2$ emissions. At higher loading conditions (80% and 100% load), the $CO_2$ emissions increased due to an increase in unburned HC. The complete combustion of hydrocarbons produces $CO_2$ and $H_2O$ (vapor). Figure 19 shows the variation in $CO_2$ emissions and the brake power of test fuel blends.
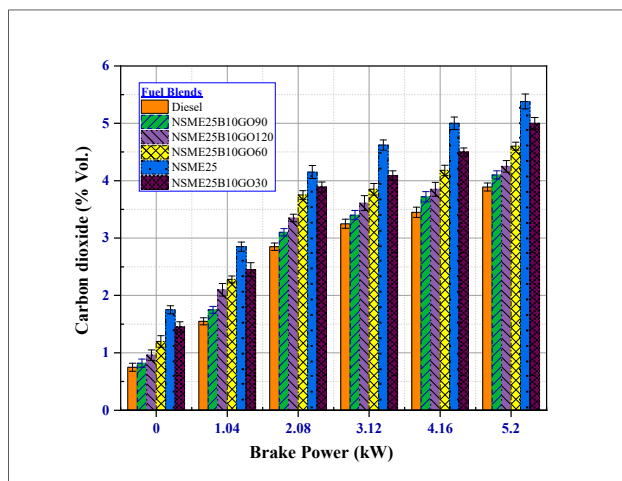
**Figure 19.** Variation of NOx emissions and brake power for test fuel blends.

Adding 10% n-butanol to the blend of fuel increases the combustion process at lower engine and combustion temperatures [48,54]. At higher loads and combustion rates producing more $CO_2$ emissions, the $CO_2$ emissions for the NSME25B10GO90 fuel blend were comparable with the diesel fuel, indicating complete fuel combustion due to improved oxidation. At 100% load, the $CO_2$ emissions for NSME25B10GO90, NSME25B10GO120, NSME25B10GO60 and NSME25B10GO30 nanofuel blends were reduced compared to NSME25. The *Nigella sativa* biodiesel (NSME25) produced the highest $CO_2$ emissions due to the incomplete combustion of this fuel blend.

### 4.3.5. Effect of Fuel Additives on Smoke Emissions

Graphene oxide nanoparticles have a large asymmetric surface area of180 $m^2$/g, and therefore act as an activated reaction site for air and fuel molecules [3]. Figure 20 shows variations in smoke emissions and brake power for fuel test blends. The higher thermal conductivity of graphene oxide NPs (5000 W/mK) allows the nanoparticles to transfer sufficient heat to individual molecules of the combustion product placed on the additive surface and thus enhances the oxidation of carbonaceous particles. Additionally, the inherent properties of Butanol (10%), such as higher oxygen content, lower viscosity and lower BP lead to enhanced combustion characteristics through improved atomization, reducing the smoke emissions [48].
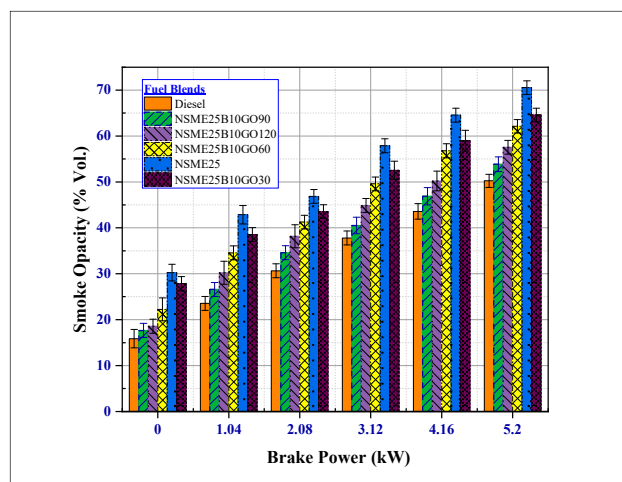


**Figure 20.** Variation of in-cylinder temperature and crank angle for different fuel blends.

At maximum loads, the smoke emissions increase due to a large quantity of smoke entering the combustion chamber. For maximum load, the smoke emissions for NSME25B10GO90 and NSME25B10GO120 nanofuel blends were 31.68% (53.85 HSU) and 22.54% (57.55 HSU) lower when compared with NSME25 (70.55 HSU); fuel and smoke emissions for NSME25B10GO90 were comparable to neat diesel fuel. The lower ID period of the nanofuel blends also resulted in a faster premixed combustion phase, which caused a reduction in smoke emissions.

## 5. Response Surface Methodology of Nanofuel Blends

In Figure 21, the fuel blends (1 to 6) represent (1) pure diesel, (2) NSME, (3) NSME25B10GO30, (4) NSME25B10GO60, (5) NSME25B10GO90, and (6) NSME25B10GO120. The contour plot of BTE shows that, for BP = 0, BTE = 0, for all the blends. As the BP increases, the region of BTE slowly increases and the asymmetric region of maximum BTE is observed in the zone of BP 4 and 5. Figure 21a indicates that the BTE increases with the increase in BP, but the maximum zone is observed for neat diesel and blends with 120 ppm of GO.
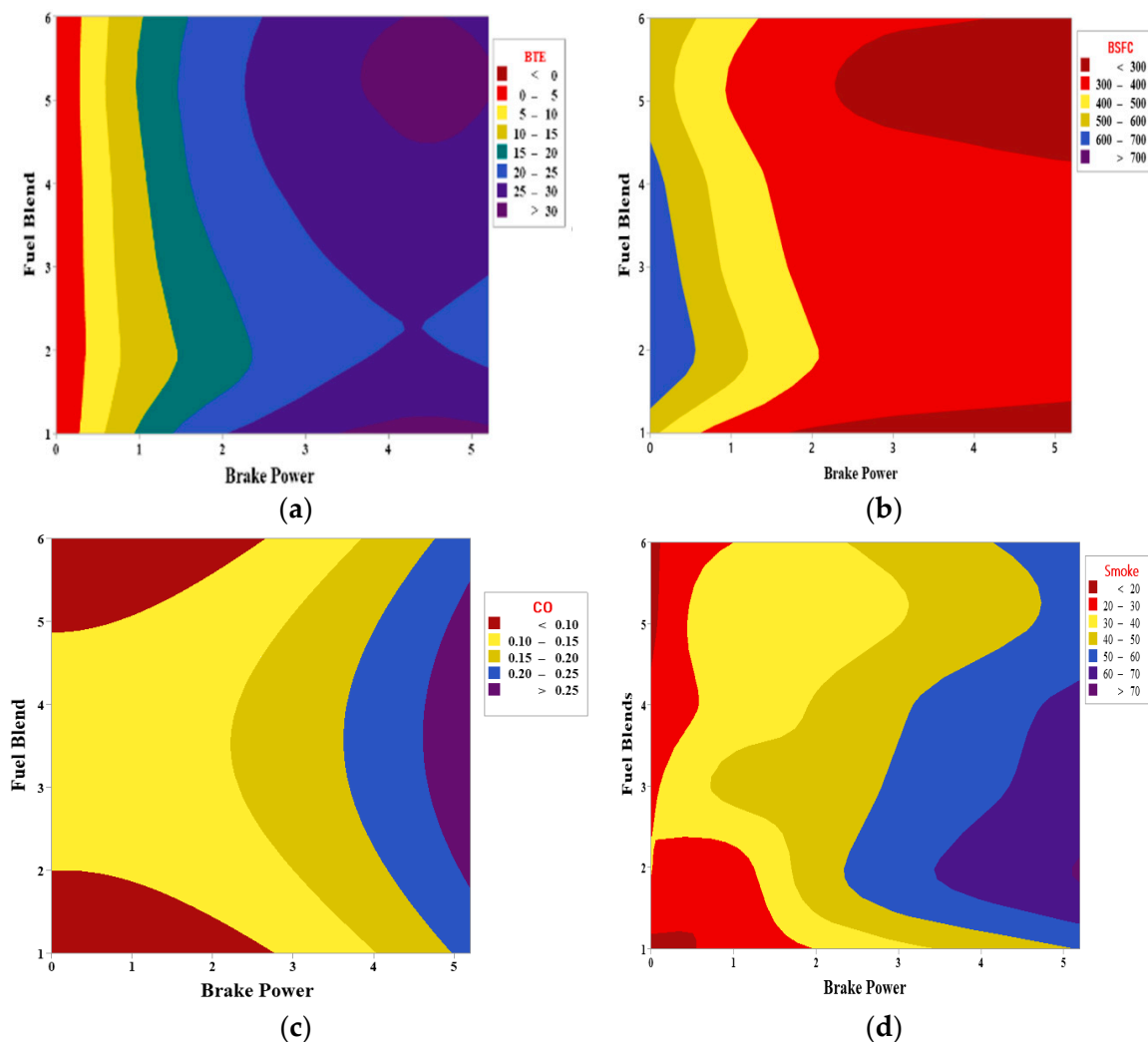


**Figure 21.** Illustration of: (**a**) BTE and (**b**) BSFC as a function of brake power, and blends' (**c**) zone of high CO emission at BP > 5 and fuel blends with lower GO concentrations and (**d**) smoke emissions.

For pure Nigella oil, the BTE is lowest of all. In Figure 21d, the smoke emissions for all blends are depicted. The BP influences the increase in smoke emission from the engine. At BP < 3 the smoke emission is minimal. Only for pure Nigella oil at BP>5 is the zone of maximum emission observed. The presence of GO nanoparticles with a 120-ppm concentration leads the emissions to

reduce. This zone starts with the addition of GO nanoparticles and ends at a minimal point at the right top corner. Tables 6 and 7 illustrate the regression equations in uncoded units and the model summary.

**Table 6.** Regression equation in uncoded units.

| |
|---|
| BTE = 4.35 + 13.519 BP − 2.790 Blend − 1.645 BP*BP + 0.410 Blend*Blend + 0.043 BP*Blend |
| BSFC = 503.6 − 156.8 BP + 75.2 Blend + 19.43 BP*BP − 10.85 Blend*Blend − 0.10 BP*Blend |
| CO = −0.0009 − 0.0040 BP + 0.0713 Blend + 0.00630 BP*BP − 0.01041 Blend*Blend + 0.00083 BP*Blend |
| Smoke = 6.36 + 9.57 BP + 11.73 Blend − 0.368 BP*BP − 1.637 Blend*Blend − 0.156 BP*Blend |

**Table 7.** Model summary.

| | S | R-sq | R-sq(adj) | R-sq(pred) |
|---|---|---|---|---|
| Smoke | 5.46660 | 87.71% | 85.66% | 82.51% |
| CO | 0.0390499 | 76.49% | 72.57% | 65.10% |
| BTE | 1.97657 | 96.95% | 96.44% | 95.37% |
| BSFC | 45.0148 | 88.82% | 86.96% | 83.43% |

In Figure 21c the CO emission is quite clear and indicates that the lowest CO emissions are for either diesel at the lowest BP or for Nigella oil with 90 and 120 ppm of GO nanoparticles. The maximum zone of CO emissions is at BP > 5, and for oil with lower concentrations (30 to 60 ppm) of NPs. The zone shown in yellow has covers a larger area and shows an acceptable amount of CO emissions at BP ranging from 0 to 4 kW. Hence, the CO emissions can be observed to be at the safest point for BP 0 to 4 kW and all fuel blends, while pure diesel and oil with 120 ppm at minimum load are best. It can also be said that, for high BP loads, the addition of less quantity of nanoparticles does not have any positive side effect; rather, the emission character of the diesel engine deteriorates. n-butanol also combusts very easily compared with biodiesel due to the high cetane number; thus, it is the most suitable oxygenated liquid fuel additive [59,63,64].

## 6. Conclusions

Experimental investigations were conducted on the CRDI engine; the toroidal combustion chamber and a six-hole fuel injector were used in this investigation. An oxygenated additive, n-butanol (10%), was added to reduce the viscosity and increase the cetane number of the biodiesel and graphene oxide nanoparticles; this increases the micro-explosion phenomenon and acts as a catalyst. In this section, the effects of *Nigella sativa* biodiesel (NSME25) blended with diesel, n-butanol, and asymmetric graphene oxide nanoparticles on modified CRDI engine are summarized:

1.  The NSME25, n-butanol and graphene oxide nanoparticle emulsion fuel illustrated an enhanced BTE value compared to the NSME (B25) fuel blend; the BTE of NSME25B10GO90 was nearly equivalent to diesel fuel. For NSME25B10GO90 fuel, the BTE increased by 18.37% compared to the NSME25. The enhancement in the BTE for all nanofuel blends is due to the catalytic effect of GO NPs.
2.  In addition, the BSFC values for all nanofuel blends with n-butanol decreased due to complete fuel combustion and an improved A: F mixing ratio; this is due to excess oxygen atoms in the combustion chamber and higher in-cylinder temperature.
3.  The toroidal combustion chamber demonstrated better A:F mixing due to an enhanced swirling motion and six-hole fuel injector at an injection pressure of 900 bar; this led to an instantaneous combustion, which improved the heat release rate and cylinder pressure.
4.  The NOx emissions for the NSME25, n-butanol and GO NPs fuel blend increased due to surplus oxygen molecules present in the combustion chamber and high combustion chamber temperature; lower NOx emissions were observed for NSME25 and diesel fuel. Meanwhile, the NSME25B10GO120 emitted maximum NOx emissions at all loads.

5. The addition of GO NPs to the *Nigella sativa* reduced all the other noxious emissions ($CO_2$, HC, smoke, and CO). At maximum load, NSME25B10GO90 fuel blend smoke, HC and CO emissions decreased by 31.68%, 48.571% and 50.15% compared with NSME25 fuel blend.

6. The enhancement of the BTE increased the EGT for diesel and nanofuel blend, leading to rapid combustion of fuel blends, and lowered the ignition delay at maximum load shortly after the SOC period.

The experimental investigation recommends that the addition of high concentrations of graphene oxide nanoparticles, 90 and 120 ppm and 10% n-butanol in *Nigella sativa* biodiesel improves the overall CRDI engine characteristics, in symmetry with preceding research. Additionally, the toroidal combustion chamber and six-hole fuel injector nozzle with an orifice diameter of 0.1 mm increases the swirl motion and high-pressure impingement of fuel spray for a rapid combustion of fuel.

**Author Contributions:** H.K.: Conceptualization, Methodology, Investigation, Writing-Original Draft; M.E.M.S.: Design of the study; Conceptualization, Writing Methodology, and Reviewing; R.H.K.: Supervision and Project administration; M.R.S.: Project administration, Writing, Review & Editing; M.F.: Formal analyses and Reviewing; A.K.: Interpretation of results, Review & Editing; N.R.B.: Supervision, Project administration and Resources; R.A.F.: Review & Editing; M.M.A.: Disussion of Results and interpretation of data; A.A.: Design and Analysis, Data interpretation; W.A.: Validation of results; M.G.: Review & Editing, Supervision; S.N.T.: Review & Editing, Formal analysis. All authors have read and agreed to the published version of the manuscript.

**Conflicts of Interest:** The authors declare no conflict of interest.

## Nomenclature

| | | | |
|---|---|---|---|
| **NPs** | Nanoparticles | **GO** | Graphene oxide |
| **CRDI** | Common rail direct injection | **SDBS** | Sodium dodecyl benzene sulphonate |
| **CI** | Compression ignition | **IC** | Internal combustion |
| **nm** | Nanometer | **A: F** | Air-to-fuel ratio |
| **g/kWh** | Grams per kilowatt hour | **ppm** | Parts per million |
| **CC** | Combustion chamber | **m** | Meter |
| **ATDC** | After top dead centre | **TCC** | Toroidal combustion chamber |
| **FFA** | Free fatty acid | **BTDC** | Before top dead centre |
| **A:F** | Air Fuel mixture | **CR** | Compression ratio |
| **ID** | Injection delay | **PP** | Peak cylinder pressure |
| **CO$_2$** | Carbon dioxide | **HC** | Hydrocarbon |
| **NO$_X$** | Oxides of nitrogen | **CO** | Carbon monoxide |
| **BTE** | Brake thermal efficiency | **PM** | Particulate matter |
| **SFC** | Specific fuel consumption | **BSFC** | Brake-specific fuel consumption |
| **max.** | Maximum | **vol** | Volume |
| **T** | Temperature | **P** | Pressure |
| **ASTM** | American Society for Testing and Materials | **T$_w$** | Wall temperature |
| **CN** | Cetane number | **η$_{th}$** | Thermal efficiency |
| **IP** | Injection pressure | **IT** | Injection timing |
| **EGT** | Exhaust gas temperature | **HRR** | Heat release rate |
| **CD** | Combustion duration | **CP** | Cylinder pressure |
| **°CA** | Crank angle (degrees) | **D100** | 100% diesel |
| **NSME** | *Nigella sativa* methyl ester (Nigella biodiesel) | **NSME25** | 25% *Nigella sativa* methyl ester blended with diesel |
| **NSME25 B10GO30** | NSME25 with 10% n-butanol and 30 ppm GO NPs | **NSME25 B10GO60** | NSME25 with 10% n-butanol and 60 ppm GO NPs |
| **NSME25 B10GO90** | NSME25 with 10% n-butanol and 90 ppm GO NPs | **NSME25 B10GO120** | NSME25 with 10% n-butanol and 120 ppm GO NPs |

# References

1. Soudagar, M.E.M.; Nik-Ghazali, N.N.; Kalam, M.A.; Badruddin, I.A.; Banapurmath, N.R.; Akram, N. The effect of nano-additives in diesel-biodiesel fuel blends: A comprehensive review on stability, engine performance and emission characteristics. *Energy Convers. Manag.* **2018**, *178*, 146–177. [CrossRef]

2. Soudagar, M.E.M.; Nik-Ghazali, N.N.; Kalam, M.A.; Badruddin, I.A.; Banapurmath, N.R.; Ali, M.A.B.; Kamangar, S.; Cho, H.M.; Akram, N. An investigation on the influence of aluminium oxide nano-additive and honge oil methyl ester on engine performance, combustion and emission characteristics. *Renew. Energy* **2020**, *146*, 2291–2307. [CrossRef]

3. Soudagar, M.E.M.; Nik-Ghazali, N.N.; Kalam, M.A.; Badruddin, I.A.; Banapurmath, N.R.; Khan, T.Y.; Bashir, M.N.; Akram, N.; Farade, R.; Afzal, A. The effects of graphene oxide nanoparticle additive stably dispersed in dairy scum oil biodiesel-diesel fuel blend on CI engine: Performance, emission and combustion characteristics. *Fuel* **2019**, *257*, 116015. [CrossRef]

4. Aghabarari, B.; Dorostkar, N.; Martinez-Huerta, M. Synthesis of biodiesel from *Nigella sativa* seed oil using surfactant-Brønsted acidic-combined ionic liquid as catalyst. *Fuel Process. Technol.* **2014**, *118*, 296–301. [CrossRef]

5. Atabani, A.E.; Silitonga, A.S.; Badruddin, I.A.; Mahlia, T.M.I.; Masjuki, H.H.; Mekhilef, S. A comprehensive review on biodiesel as an alternative energy resource and its characteristics. *Renew. Sustain. Energy Rev.* **2012**, *16*, 2070–2093. [CrossRef]

6. Atabani, A.E.; Silitonga, A.S.; Ong, H.C.; Mahlia, T.M.I.; Masjuki, H.H.; Badruddin, I.A.; Fayaz, H. Non-edible vegetable oils: A critical evaluation of oil extraction, fatty acid compositions, biodiesel production, characteristics, engine performance and emissions production. *Renew. Sustain. Energy Rev.* **2013**, *18*, 211–245. [CrossRef]

7. Soudagar, M.E.M.; Kittur, P.; Parmar, F.; Batakatti, S.; Kulkarni, P.; Kallannavar, V. Production of jath Oil Ethyl Ester (MOEE) and its Performance test on four stroke single cylinder VCR engine. In *IOP Conference Series: Materials Science and Engineering*; IOP Publishing: Philadelphia, PA, USA, 2017; Volume 225, p. 012029.

8. Azam, M.M.; Waris, A.; Nahar, N. Prospects and potential of fatty acid methyl esters of some non-traditional seed oils for use as biodiesel in India. *Biomass Bioenergy* **2005**, *29*, 293–302.

9. Delvi, M.K.; Soudagar, M.E.M.; Khan, H.; Ahmed, Z.; Shariff, I.M. Biodiesel Production Utilizing Diverse Sources, Classification of Oils and Their Esters, Performance and Emission Characteristics: A Research. *IJRTE* **2020**. [CrossRef]

10. Soudagar, M.E.M.; Nik-Ghazali, N.N.; Badruddin, I.A.; Kalam, M.A.; Kittur, M.I.; Akram, N.; Ullah, M.A.; Khan, T.Y.; Mokashi, I. Production of honge oil methyl ester (HOME) and its performance test on four stroke single cylinder VCR engine. In *AIP Conference Proceedings*; AIP Publishing LLC: New York, NY, USA, 2019; Volume 2142, p. 200006.

11. Sheriff, S.A.; Kumar, I.K.; Mandhatha, P.S.; Jambal, S.S.; Sellappan, R.; Ashok, B.; Nanthagopal, K. Emission reduction in CI engine using biofuel reformulation strategies through nano additives for atmospheric air quality improvement. *Renew. Energy* **2020**, *147*, 2295–2308. [CrossRef]

12. Mujtaba, M.A.; Cho, H.M.; Masjuki, H.H.; Kalam, M.A.; Ong, H.C.; Gul, M.; Harith, M.H.; Yusoff, M.N.A.M. Critical review on sesame seed oil and its methyl ester on cold flow and oxidation stability. *Energy Rep.* **2020**, *6*, 40–54. [CrossRef]

13. Achten, W.M.; Mathijs, E.; Verchot, L.; Singh, V.P.; Aerts, R.; Muys, B. Jatropha biodiesel fueling sustainability? *Biofuels Bioprod. Biorefin. Innov. Sustain. Econ.* **2007**, *1*, 283–291. [CrossRef]

14. Heidari-Maleni, A.; Gundoshmian, T.M.; Jahanbakhshi, A.; Ghobadian, B. Performance improvement and exhaust emissions reduction in diesel engine through the use of graphene quantum dot (GQD) nanoparticles and ethanol-biodiesel blends. *Fuel* **2020**, *267*, 117116. [CrossRef]

15. Basha, J.S. Impact of Carbon Nanotubes and Di-Ethyl Ether as additives with biodiesel emulsion fuels in a diesel engine—An experimental investigation. *J. Energy Inst.* **2018**, *91*, 289–303. [CrossRef]

16. Akram, N.; Sadri, R.; Kazi, S.N.; Zubir, M.N.M.; Ridha, M.; Ahmed, W.; Soudagar, M.E.M.; Arzpeyma, M. A comprehensive review on nanofluid operated solar flat plate collectors. *J. Therm. Anal. Calorim.* **2020**, *139*, 1309–1343. [CrossRef]

17. Ooi, J.B.; Ismail, H.M.; Swamy, V.; Wang, X.; Swain, A.K.; Rajanren, J.R. Graphite oxide nanoparticle as a diesel fuel additive for cleaner emissions and lower fuel consumption. *Energy Fuels* **2016**, *30*, 1341–1353. [CrossRef]

18. Kim, F.; Luo, J.; Cruz-Silva, R.; Cote, L.J.; Sohn, K.; Huang, J. Self-propagating domino-like reactions in oxidized graphite. *Adv. Funct. Mater.* **2010**, *20*, 2867–2873. [CrossRef]

19. Mauter, M.S.; Elimelech, M. Environmental applications of carbon-based nanomaterials. *Environ. Sci. Technol.* **2008**, *42*, 5843–5859. [CrossRef]

20. Hosseini, S.H.; Taghizadeh-Alisaraei, A.; Ghobadian, B.; Abbaszadeh-Mayvan, A. Performance and emission characteristics of a CI engine fuelled with carbon nanotubes and diesel-biodiesel blends. *Renew. Energy* **2017**, *111*, 201–213. [CrossRef]

21. Venkateswaran, S.P.; Nagarajan, G. Effects of the re-entrant bowl geometry on a DI turbocharged diesel engine performance and emissions—A CFD approach. *J. Eng. Gas Turbines Power* **2010**, *132*. [CrossRef]

22. Bapu, B.R.; Saravanakumar, L.; Prasad, B.D. Effects of combustion chamber geometry on combustion characteristics of a DI diesel engine fueled with *calophyllum inophyllum* methyl ester. *J. Energy Inst.* **2017**, *90*, 82–100. [CrossRef]

23. Hoseini, S.S.; Najafi, G.; Ghobadian, B.; Mamat, R.; Ebadi, M.T.; Yusaf, T. Novel environmentally friendly fuel: The effects of nanographene oxide additives on the performance and emission characteristics of diesel engines fuelled with Ailanthus altissima biodiesel. *Renew. Energy* **2018**, *125*, 283–294. [CrossRef]

24. EL-Seesy, A.I.; Hassan, H.; Ookawara, S. Performance, combustion, and emission characteristics of a diesel engine fueled with Jatropha methyl ester and graphene oxide additives. *Energy Convers. Manag.* **2018**, *166*, 674–686. [CrossRef]

25. Hoseini, S.S.; Najafi, G.; Ghobadian, B.; Ebadi, M.T.; Mamat, R.; Yusaf, T. Biodiesels from three feedstock: The effect of graphene oxide (GO) nanoparticles diesel engine parameters fuelled with biodiesel. *Renew. Energy* **2020**, *145*, 190–201. [CrossRef]

26. Ooi, J.B.; Ismail, H.M.; Tan, B.T.; Wang, X. Effects of graphite oxide and single-walled carbon nanotubes as diesel additives on the performance, combustion, and emission characteristics of a light-duty diesel engine. *Energy* **2018**, *161*, 70–80. [CrossRef]

27. Debbarma, S.; Misra, R.D.; Das, B. Performance of graphene-added palm biodiesel in a diesel engine. *Clean Technol. Environ. Policy* **2020**, 1–12. [CrossRef]

28. Paramashivaiah, B.M.; Banapurmath, N.R.; Rajashekhar, C.R.; Khandal, S.V. Studies on effect of graphene nanoparticles addition in different levels with simarouba biodiesel and diesel blends on performance, combustion and emission characteristics of CI engine. *Arab. J. Sci. Eng.* **2018**, *43*, 4793–4801. [CrossRef]

29. Khan, T.Y.; Atabani, A.E.; Badruddin, I.A.; Ankalgi, R.F.; Khan, T.M.; Badarudin, A. Ceiba pentandra, *Nigella sativa* and their blend as prospective feedstocks for biodiesel. *Ind. Crops Prod.* **2015**, *65*, 367–373. [CrossRef]

30. Ahmad, A.; Husain, A.; Mujeeb, M.; Khan, S.A.; Najmi, A.K.; Siddique, N.A.; Damanhouri, Z.A.; Anwar, F. A review on therapeutic potential of *Nigella sativa*: A miracle herb. *Asian Pac. J. Trop. Biomed.* **2013**, *3*, 337–352. [CrossRef]

31. Goreja, W. *Black Seed: Nature's Miracle Remedy*; Karger Publishers: Basel, Switzerland, 2003.

32. Encyclopaedia *Britannica*. Black cumin. In *Black Cumin—PLANT AND SEED*; Encyclopædia Britannica, Inc.: Chicago, IL, USA, 2018; Available online: https://www.britannica.com/plant/black-cumin (accessed on 6 May 2020).

33. Ain, Q.T.; Haq, S.H.; Alshammari, A.; Al-Mutlaq, M.A.; Anjum, M.N. The systemic effect of PEG-nGO-induced oxidative stress in vivo in a rodent model. *Beilstein J. Nanotechnol.* **2019**, *10*, 901–911. [CrossRef]

34. Farade, A.R.; Wahab, N.I.B.A.; Mansour, D.E.A.; Azis, N.B.; Banapurmath, N.R.; Soudagar, M.E.M. Investigation of the dielectric and thermal properties of non-edible cottonseed oil by infusing h-BN nanoparticles. *IEEE Access* **2020**. [CrossRef]

35. Wilson, N.R.; Pandey, P.A.; Beanland, R.; Young, R.J.; Kinloch, I.A.; Gong, L.; Liu, Z.; Suenaga, K.; Rourke, J.P.; York, S.J.; et al. Graphene oxide: Structural analysis and application as a highly transparent support for electron microscopy. *ACS Nano* **2009**, *3*, 2547–2556. [CrossRef] [PubMed]

36. Rakopoulos, D.; Rakopoulos, C.D.; Giakoumis, G.; Dimaratos, M.; Kyritsis, C. Effects of butanol—Diesel fuel blends on the performance and emissions of a high-speed DI diesel engine. *Energy Convers. Manag.* **2010**, *51*, 1989–1997. [CrossRef]

37. Chen, Z.; Liu, J.; Han, Z.; Du, B.; Liu, Y.; Lee, C. Study on performance and emissions of a passenger-car diesel engine fueled with butanol—Diesel blends. *Energy* **2013**, *55*, 638–646. [CrossRef]

38. Ibrahim, A. Performance and combustion characteristics of a diesel engine fuelled by butanol—Biodiesel—diesel blends. *Appl. Therm. Eng.* **2016**, *103*, 651–659. [CrossRef]

39. Al-Samaraae, R.; Atabani, A.E.; Uguz, G.; Kumar, G.; Arpa, O.; Ayanoglu, A.; Mohammed, M.N.; Farouk, H. Perspective of safflower (Carthamus tinctorius) as a potential biodiesel feedstock in Turkey: Characterization, engine performance and emissions analyses of butanol—Biodiesel—diesel blends. *Biofuels* **2017**, 1–17. [CrossRef]

40. Ashok, B.; Nanthagopal, K.; Saravanan, B.; Somasundaram, P.; Jegadheesan, C.; Chaturvedi, B.; Sharma, S.; Patni, G. A novel study on the effect lemon peel oil as a fuel in CRDI engine at various injection strategies. *Energy Convers. Manag.* **2018**, *172*, 517–528. [CrossRef]

41. Örs, I.; Sarıkoç, S.; Atabani, A.E.; Ünalan, S.; Akansu, S.O. The effects on performance, combustion and emission characteristics of DICI engine fuelled with $TiO_2$ nanoparticles addition in diesel/biodiesel/n-butanol blends. *Fuel* **2018**, *234*, 177–188.

42. Hawi, M.; Elwardany, A.; Ismail, M.; Ahmed, M. Experimental investigation on performance of a compression ignition engine fueled with waste cooking oil biodiesel–diesel blend enhanced with iron-doped cerium oxide nanoparticles. *Energies* **2019**, *12*, 798. [CrossRef]

43. Banapurmath, N.R.; Sankaran, R.; Tumbal, A.V.; TN, N.; Hunashyal, A.M.; Ayachit, N.H. Experimental investigation on direct injection diesel engine fuelled with graphene, silver and multiwalled carbon nanotubes-biodiesel blended fuels. *Int. J. Automot. Eng. Technol.* **2014**, *3*, 129–138. [CrossRef]

44. Javed, S.; Murthy, Y.S.; Satyanarayana, M.R.S.; Reddy, R.R.; Rajagopal, K. Effect of a zinc oxide nanoparticle fuel additive on the emission reduction of a hydrogen dual-fuelled engine with jatropha methyl ester biodiesel blends. *J. Clean. Prod.* **2016**, *137*, 490–506. [CrossRef]

45. Ahmed, A.; Shah, A.N.; Azam, A.; Uddin, G.M.; Ali, M.S.; Hassan, S.; Ahmed, H.; Aslam, T. Environment-friendly novel fuel additives: Investigation of the effects of graphite nanoparticles on performance and regulated gaseous emissions of CI engine. *Energy Convers. Manag.* **2020**, *211*, 112748. [CrossRef]

46. Fatah, M.A.; Farag, H.; Ossman, M. Production of biodiesel from non-edible oil and effect of blending with diesel on fuel properties. *Eng. Sci. Technol. Int. J.* **2012**, *2*, 583–591.

47. Nanthagopal, K.; Ashok, B.; Tamilarasu, A.; Johny, A.; Mohan, A. Influence on the effect of zinc oxide and titanium dioxide nanoparticles as an additive with *Calophyllum inophyllum* methyl ester in a CI engine. *Energy Convers. Manag.* **2017**, *146*, 8–19. [CrossRef]

48. El-Seesy, A.I.; Hassan, H. Investigation of the effect of adding graphene oxide, graphene nanoplatelet, and multiwalled carbon nanotube additives with n-butanol-Jatropha methyl ester on a diesel engine performance. *Renew. Energy* **2019**, *132*, 558–574. [CrossRef]

49. Gupta, H.N. *Fundamentals of Internal Combustion Engines*; PHI Learning Pvt. Ltd.: New Delhi, India, 2012.

50. El-Seesy, A.I.; Abdel-Rahman, A.K.; Bady, M.; Ookawara, S.J.E.C. Performance, combustion, and emission characteristics of a diesel engine fueled by biodiesel-diesel mixtures with multi-walled carbon nanotubes additives. *Energy Convers. Manag.* **2017**, *135*, 373–393. [CrossRef]

51. Annamalai, M.; Dhinesh, B.; Nanthagopal, K.; Sivarama Krishnan, P.; Lalvani, J.I.J.; Parthasarathy, M.; Annamalai, K. An assessment on performance, combustion and emission behavior of a diesel engine powered by ceria nanoparticle blended emulsified biofuel. *Energy Convers. Manag.* **2016**, *123*, 372–380. [CrossRef]

52. Aalam, C.S.; Saravanan, C.; Kannan, M. Experimental investigations on a CRDI system assisted diesel engine fuelled with aluminium oxide nanoparticles blended biodiesel. *Alex. Eng. J.* **2015**, *54*, 351–358. [CrossRef]

53. Imdadul, H.K.; Masjuki, H.H.; Kalam, M.A.; Zulkifli, N.W.M.; Kamruzzaman, M.; Shahin, M.M.; Rashed, M.M. Evaluation of oxygenated n-butanol-biodiesel blends along with ethyl hexyl nitrate as cetane improver on diesel engine attributes. *J. Clean. Prod.* **2017**, *141*, 928–939. [CrossRef]

54. Altun, S.; Oner, C.; Yasar, F.; Adin, H. Effect of n-butanol blending with a blend of diesel and biodiesel on performance and exhaust emissions of a diesel engine. *Ind. Eng. Chem. Res.* **2011**, *50*, 9425–9430. [CrossRef]

55. Mirzajanzadeh, M.; Tabatabaei, M.; Ardjmand, M.; Rashidi, A.; Ghobadian, B.; Barkhi, M.; Pazouki, M. A novel soluble nano-catalysts in diesel–biodiesel fuel blends to improve diesel engines performance and reduce exhaust emissions. *Fuel* **2015**, *139*, 374–382. [CrossRef]

56. Yesilyurt, M.K.; Aydin, M. Experimental investigation on the performance, combustion and exhaust emission characteristics of a compression-ignition engine fueled with cottonseed oil biodiesel/diethyl ether/diesel fuel blends. *Energy Convers. Manag.* **2020**, *205*, 112355. [CrossRef]

57. Nanthagopal, K.; Kishna, R.S.; Atabani, A.E.; Ala'a, H.; Kumar, G.; Ashok, B. A compressive review on the effects of alcohols and nanoparticles as an oxygenated enhancer in compression ignition engine. *Energy Convers. Manag.* **2020**, *203*, 112244. [CrossRef]

58. Watson, A.Y.; Richard, R.B.; Kennedy, D. (Eds.) *Air Pollution, the Automobile, and Public Health*; National Academies: Washington, DC, USA, 1988.

59. Hoseini, S.S.; Najafi, G.; Ghobadian, B.; Ebadi, M.T.; Mamat, R.; Yusaf, T. Performance and emission characteristics of a CI engine using graphene oxide (GO) nano-particles additives in biodiesel-diesel blends. *Renew. Energy* **2020**, *145*, 458–465. [CrossRef]

60. Vairamuthu, G.; Sundarapandian, S.; Kailasanathan, C.; Thangagiri, B. Experimental investigation on the effects of cerium oxide nanoparticle on *Calophyllum inophyllum* (Punnai) biodiesel blended with diesel fuel in DI diesel engine modified by nozzle geometry. *J. Energy Inst.* **2016**, *89*, 668–682. [CrossRef]

61. Khalife, E.; Tabatabaei, M.; Najafi, B.; Mirsalim, S.M.; Gharehghani, A.; Mohammadi, P.; Aghbashlo, M.; Ghaffari, A.; Khounani, Z.; Shojaei, T.R.; et al. A novel emulsion fuel containing aqueous nano cerium oxide additive in diesel–biodiesel blends to improve diesel engines performance and reduce exhaust emissions: Part I–Experimental analysis. *Fuel* **2017**, *207*, 741–750. [CrossRef]

62. Zeldovich, Y.; Frank-Kamenetskii, D.; Sadovnikov, P. *Oxidation of Nitrogen in Combustion*; Publishing House of the Acad of Sciences of USSR: Moscow, Russia, 1947.

63. Szwaja, S.; Naber, J.D. Combustion of n-butanol in a spark-ignition IC engine. *Fuel* **2010**, *89*, 1573–1582. [CrossRef]

64. Soudagar, M.; Afzal, A.; Kareemullah, M. Waste coconut oil methyl ester with and without additives as an alternative fuel in diesel engine at two different injection pressures. *Energy Sources Part A Recovery Util. Environ. Eff.* **2020**. [CrossRef]